JYVÄSKYLÄ STUDIES IN BIOLOGICAL AND ENVIRONMENTAL SCIENCE
334

Marie Stark

Recombinant Nanocapsid for Targeted Theranostic Delivery

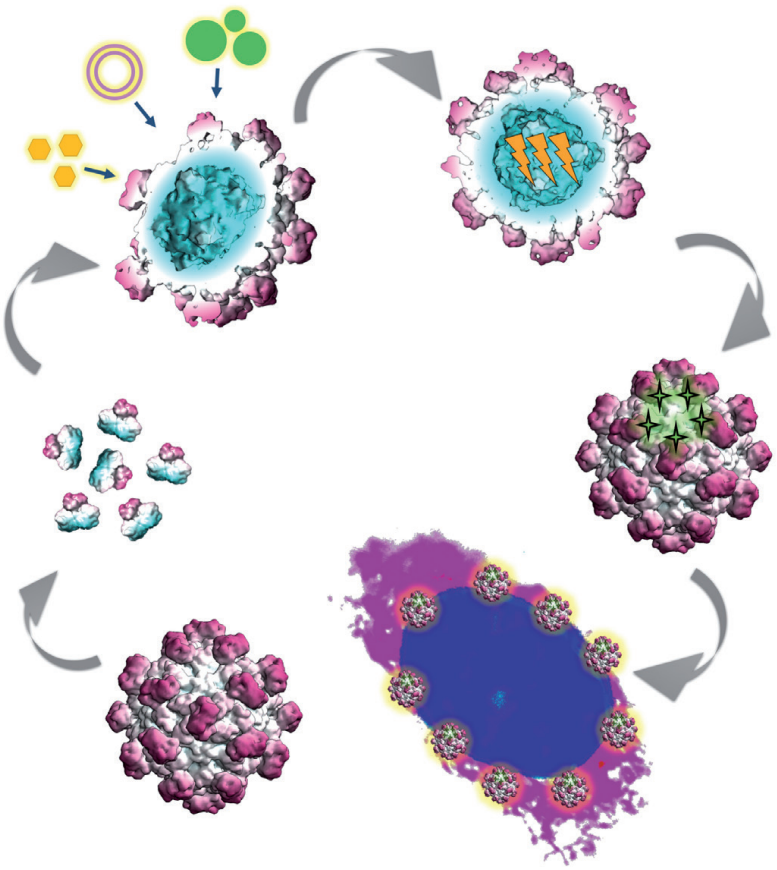

JYVÄSKYLÄN YLIOPISTO

JYVÄSKYLÄ STUDIES IN BIOLOGICAL AND ENVIRONMENTAL SCIENCE 334

Marie Stark

Recombinant Nanocapsid for Targeted Theranostic Delivery

Esitetään Jyväskylän yliopiston matemaattis-luonnontieteellisen tiedekunnan suostumuksella
julkisesti tarkastettavaksi yliopiston Ambiotica-rakennuksen salissa YAA303,
kesäkuun 17. päivänä 2017 kello 12.

Academic dissertation to be publicly discussed, by permission of
the Faculty of Mathematics and Science of the University of Jyväskylä,
in building Ambiotica, hall YAA303, on June 17, 2017 at 12 o'clock noon.

UNIVERSITY OF JYVÄSKYLÄ

JYVÄSKYLÄ 2017

Recombinant Nanocapsid for Targeted Theranostic Delivery

JYVÄSKYLÄ STUDIES IN BIOLOGICAL AND ENVIRONMENTAL SCIENCE 334

Marie Stark

Recombinant Nanocapsid for Targeted Theranostic Delivery

UNIVERSITY OF JYVÄSKYLÄ

JYVÄSKYLÄ 2017

Editors
Varpu Marjomäki
Department of Biological and Environmental Science, University of Jyväskylä
Pekka Olsbo, Ville Korkiakangas
Publishing Unit, University Library of Jyväskylä

Jyväskylä Studies in Biological and Environmental Science
Editorial Board

Jari Haimi, Anssi Lensu, Timo Marjomäki, Varpu Marjomäki
Department of Biological and Environmental Science, University of Jyväskylä

Cover picture by Marie Stark and Mo Baikoghli.

Permanent link to this publication: http://urn.fi/URN:ISBN:978-951-39-7118-2

URN:ISBN:978-951-39-7118-2
ISBN 978-951-39-7118-2 (PDF)

ISBN 978-951-39-7117-5 (nid.)
ISSN 1456-9701

Jyväskylä University Printing House, Jyväskylä 2017

ABSTRACT

Stark, Marie
Recombinant Nanocapsid for Targeted Theranostic Delivery
Jyväskylä: University of Jyväskylä, 2017, 72 p.
(Jyväskylä Studies in Biological and Environmental Science
ISSN 1456-9701; 334)
ISBN 978-951-39-7117-5 (nid.)
ISBN 978-951-39-7118-2 (PDF)
Yhteenveto: Nanokapsidien kehittely kohdennettavia lääkehoitoja varten
Diss.

Developments in diagnostic and therapeutic delivery are trending towards molecular level targeting with nano-platforms. Targeted delivery reduces generalized distribution by localizing diagnostic and/or therapeutic (theranostic) molecules to an intended target site. The first section of this thesis proposes Hepatitis E Virus (HEV) nanocapsids as a vector to stabilize and target theranostic delivery. Derived from the capsid protein of HEV, a feco-orally transmitted virus, HEV-like particles self-assemble in to non-infectious, nanocapsids that can withstand harsh protease and pH conditions in the mucosal system. The flexible nanocapsid surface protrusion domain is amenable to substantial modification. Chemical modulation of nanocapsids was achieved through surface conjugation to single solvent exposed cysteine sites. In this thesis, nanocapsids chemically modulated with tumor-targeting ligands exhibit cancer cell-specific binding and internalization, as well as *in vivo* tumor detection. We also used cysteine sites to conjugate thiolate-protected gold nanoclusters (AuNCs), which have molecule like qualities distinct from colloidal gold nanoparticles (AuNPs). Specifically, $Au_{102}(p\text{MBA})_{44}$ (Au_{102}) and maleimide-linked Au_{102} (Au_{102}_C_6MI) were conjugated to nanocapsid cysteine through place exchange and maleimide-thiol coupling, respectively. Au_{102}_C_6MI-bound nanocapsids were imaged in cryoEM and a 3D structure was determined. The resolved structure of AuNC-bound nanocapsid revealed a 5-fold ring density attributable to AuNC densities. Rigid modelling supported this finding. In the last section of this thesis, a recombinant enterovirus was engineered to distinguish the role of structural vs. non-structural proteins in Enterovirus B infection kinetics, replication and infection persistency. The results indicated cell-receptor binding likely triggered lytic vs. non-lytic infection, providing insight in to adaptive mechanisms of native virus cell delivery.

Keywords: Bioconjugation; Gold nanocluster; Encapsulation; Enterovirus; Nanocapsid; Targeted Delivery; Theronostic

Marie Stark, University of Jyväskylä, Department of Biological and Environmental Science, P.O. Box 35, FI-40014 University of Jyväskylä, Finland

Author's address Marie Stark
Department of Biological and Environmental Science
Nanoscience Center
FI-40014 University of Jyväskylä
Finland
mcstark@ucdavis.edu
marie.c.stark@jyu.fi

Supervisors Adjunct Professor Varpu Marjomäki
Department of Biological and Environmental Science
Nanoscience Center
FI-40014 University of Jyväskylä
Finland

Academy Professor Hannu Häkkinen
Departments of Physics and Chemistry
Nanoscience Center
FI-40014 University of Jyväskylä
Finland

Professor R. Holland Cheng
Department of Molecular and Cellular Biology
Briggs Hall UC Davis Campus
1 Shields Ave
Davs, CA 95616
USA

Reviewers Associate Professor Christopher Ackerson
Department of Chemistry, Colorado State University
Ft. Collins, CO 80523
USA

Professor Mauri Kostiainen
School of Chemical Engineering
Aalto University
PO Box 11000
FI-00076 Aalto
Finland

Opponent Professor John Johnson Jr.
Department of Integrative Structural & Computational Bio.
MB-31
10500 N. Torrey Pines Road
La Jolla, CA 92037
USA

CONTENTS

LIST OF ORIGINAL PUBLICATIONS

The thesis is based on the following original papers, which will be referred to in the text by their Roman numerals.

I Chen Chun-Chieh, Xing Li, Stark Marie, Ou Tingwei, Holla Prasida, Xiao Kai, Hammock Bruce D., Lam Kit, Cheng R Holland 2016. Chemically activatable viral capsid functionalized for cancer targeting. *Nanomedicine (Lond)* 11(4), 377-390.

II Stark Marie, Cheng R. Holland 2016. Surface Modulatable Nanocapsids for Targeting and Tracking Towards Nanotheranostic Delivery 2016. *Pharmaceutical Patent Analyst (Lond)*

III Stark Marie C, Baikoghli Mo A, Lahtinen Tanja, Malola Sami, Xing Li, Nguyen Michelle, Nguyen Marina, Sikaroudi Aria, Marjomäki Varpu, Häkkinen Hannu, and Cheng R. Holland. Structural characterization of site-modulated nanocapsid with monodispersed gold clusters. Submitted to *Scientific Reports* April 28, 2017

IV Turkki Paula, Stark Marie C, Göransson Anna, Myllynen Mira, Del-Maso Heidi Sallinen, Lindberg Michael, Marjomaki Varpu. Enterovirus persistency in Rhabdomycosarcoma cells is the result of defective entry to cells. *Manuscript*

RESPONSIBILITIES

Article I — The original idea for this research was proposed by R. Holland Cheng, Li Xing, and Kit Lam. I carried out plasmid design, engineering, production, and transfection while Chun-Chieh Chen led protein production and targeting conjugation. Chun-Chieh Chen and I performed conjugation, ELISA, Western blot, and conjugation in preparation for targeting validation. Li Xing imaged HEP230-bound nanocapsid and supervised Tingwei Ou in reconstruction. Bruce D. Hammock provided the facility for insect cell work. George Kamita from the Hammock lab aided in production optimization. Kai Xiao from Lam lab performed cell and animal validation experiments. Li Xing, Prasida Holla, and I aided Chuh-Chieh Chen in writing the manuscript.

Article II — This patent review article was requested by Pharmaceutical Patent Analyst journal following the publication of our patent, *Chemically Activated Nanocapsid Functionalized for Cancer Targeting*. I prepared this review under the guidance of Professor R. Holland Cheng.

Article III — This project was first proposed by Hannu Hakkinen, Varpu Marjomaki, and R. Holland Cheng. I performed conjugation optimization, cryoEM prep/imaging, assays, and early stage single particle reconstruction (SPR). Tanja Lahtinen synthesized and assayed gold nanoclusters. Marina Nguyen and Michelle Nguyen helped me produce nanocapsids and prepare conjugations. Li Xing aided me in cryoEM imaging. Sami Malola wrote and carried out a program for rigid modeling. Aria Sikaroudi ran additional SPR to test map stability. Mo Baikoghli did PFT-hybrid reconstruction, relaxed symmetry refinement, and intensity analyses to resolve the five unique 5-fold densities. Mo helped finalize the manuscript figures. I wrote the article along with Mo, Varpu, Tanja, Sami, Hannu, and Holland.

Article IV — This project was initiated by Varpu Marjomaki and Michael Lindberg. Anna Göransson constructed chimeric and WT plasmid constructs. I carried out replicon-based virus production, purification, screening, and EM imaging. Mira Myllynen, Paula Turkki, and I performed SDS PAGE, immunolabeling and confocal imaging. Paula quantitated most of the imaging data. Mira Myllynen and Heidi Sallinen Del-Maso helped Paula with the CVB3 and CVB5 experiments. Paula Turkki wrote this together with Varpu Marjomaki and I.

ABBREVIATIONS

Ab	Antibody
AuNC	Monolayer protected gold nanocluster
AuNP	Gold nanoparticle
C_6MI	*N*-(6-hydroxyhexyl)maleimide$_n$
CAR	Coxsackie and adenovirus receptor
CPE	Cytopathic effect
CryoEM	Cryo Electron Microscopy
CPMV	Cowpei mosaic virus
CsCl	Cesium chloride
CTF	Contrast transfer function
CVB3	Coxsackievirus B3
CVB5	Coxsackievirus B5
Cys	Cysteine
DAF	Decay accelerating factor
DTT	Dithithreitol
E. coli	Escherichia coli
EDTA	Ethylenediaminetetraacetic acid
EGTA	Ethylene glyco-bis(β-aminoethyl ether)-N ,N ,N ´N ´-tetraacetic acid
EV1	Echovirus 1
EV(B)	Enterovirus (B)
EVCV	Recombinant EVB with EV1 SPs and CVB5 NSPs
Fab	Antigen binding fragment
FIB/SEM	Focused Ion Beam/ Scanning Electron Microscopy
GMK	Green monkey kidney cells
HEV	Hepatitis E Virus
Ig(A/G)	Immunoglobulin (A/G)
MES	2-ethanesulfonic acid
NHS	N-hydroxysuccinimide esters
NIR	Near infrared
NSP	Non-structural protein
ORF	Open reading frame
P (domain)	Protrusion (domain)
(d) pi	(Days) post infection
PFT	Polar fourier transform
*p*MBA	4 p-mercaptobenzoic acid
RD	Rhabdomyosarcoma cells
ScFv	Single chain variable fragment
SDS-PAGE	Sodium dodecylsulphate polyacrylamide gel
SP	Structural protein
SPR	Single particle reconstruction
TEM	Transmission electron microscopy

UV/Vis	Ultra-violet/visible spectrum
(V) LP	(Virus) Like-Particle
VP	Virus Protein
WT	*Wild type*

1 INTRODUCTION

Diseases such as cancer and genetic disorders can be difficult to detect and even harder to treat because there are no foreign pathogenic targets. Instead, something has gone awry in the patient cells, leaving dysfunctional cellular components as the target for detection and treatment. Disease heterogeneity can also make standard diagnostic tools and therapies much less reliable and effective. This has driven disease detection and management towards methods of molecular-level targeting and personalized treatment. As molecular-level targets are better understood, diagnostic and therapeutic (theranostic) agents follow suit through advancements in biotechnology. From the synergistic progress in molecular discovery and nanotechnology, an array of versatile theranostic nanoparticles have emerged. Theranostic nanoparticles are nano-sized vectors that incorporate detection, targeting, and/or therapeutics. The purpose of nanoparticles is to stabilize delivery of theranostic agents that are otherwise degraded and/or non-specifically internalized in healthy tissue. To improve theranostic strategies, biochemical interactions between nanoparticles and theranostic agents must be tuned and characterized. In addition, cell-receptor based pathways can both be investigated and targeted for specific cell binding and internalization.

This thesis outlines several applications of recombinant virus and virus-derived supramolecular complexes with the following objectives: 1.) Chemically modulate the surface of HEV-derived nanocapsids for tumor targeting and detection 2.) Characterize and determine the 3D structure of nanocapsids conjugated to gold nanocluster contrast agents 3.) Recombine structural and non-structural proteins from separate enterovirus B subspecies to identify protein domains that affect infection efficiency. The amalgamation of these efforts guides theranostic nanoparticle design and characterization, not only for targeted theranostic delivery, but also to gain insight in to cellular mechanisms to which theranostics are targeted.

2 REVIEW OF LITERATURE

2.1 Nanomedicine

2.1.1 Introduction to nanotheranostics

A fundamental understanding of disease onset and progression at the molecular level plays a pivotal role in biomedical advancement. Molecular level targeting and tuning is therefore a prevailing direction of biomedical technology. Nanomedicine uses advances in nanotechnology to study, detect, and treat disease through molecule-level targets.

Nano-sized diagnostic and therapeutic particles (theranostic) nanoparticles are on the forefront of biomedical research as multi-functional delivery agents (Farokhzad and Langer 2009, Mura and Couvreur 2012). Nanoparticles, typically between 10–1000 nm, are designed for solubility, bioavailability, low-toxicity, and physio-chemical stability (Li S.D. and Huang 2008, Caldorera-Moore *et al.* 2011). Most nanoparticles are optimized for cell uptake, resembling the size of native compounds internalized by cells. For example, 25–50 nm nanoparticles can enter cells through receptor-mediated endocytosis (RME) and vesicle uptake (Albanese *et al.* 2012). Frequently, small theranostic molecules will be degraded in the harsh physiological environment long before reaching the intended target tissue (Kang *et al.* 2015, Date *et al.* 2016). To mitigate this problem, nanoparticles can be engineered to integrate theranostic molecules and/or properties via ionic binding, recombination, conjugation or encapsulation. Nanoparticles solubilize and stabilize theranostics to improve bio-distribution, pharmacokinetics, and selective cell-internalization.

Arguably, the most profound advances in nanomedicine have been realized in cancer therapeutics. Because cancer cells are derived from originally healthy human cells, detecting and treating tumor tissue separately from healthy organs is not a trivial task. Radiation therapy works on the principle that tumor cells are more susceptible to radiation damage, because they divide more rapidly than healthy cells and because DNA repair mechanisms have been shown to be less efficient in tumor cells compared with healthy tissue (Baskar *et al.* 2014). DNA

repair is slower in tumor cells in part due to the loss of redundant DNA damage repair pathways that are present in heathy cells. Other classic therapies work on the principle that tumor cells are more sensitive to heat, such that hyperthermia treatment to heat cells between 40–43°C can induce tumor cell apoptosis, leaving healthy tissue minimally affected (Wust *et al.* 2002). Tumor tissues also exhibit increased permeability to and inefficient removal of various theranostic nanoparticles, due to an effect known as Enhanced Permeability and Retention (EPR) (Greish 2007, 2010). EPR effects result in "passive" tumor targeting, such that nanoparticle uptake is higher in tumor tissue than in healthy tissues. Therapeutic strategies relying on passive uptake, radiation, and hyperthermia are effective in some cases, but often have associated healthy tissue damage leading to severe side-effects (Lammers *et al.* 2007, Stapleton S. *et al.* 2017a, Stapleton S.J. *et al.* 2017b). It is important to note the vast tumor heterogeneity, even observed between a single cancer subtype. Moreover, cancer cells adapt in a single patient, giving rise to varying degrees of detectability and resistance to treatment. Therefore, tumor-targeted theranostic delivery, preferably in a patient specific manner, is a worthwhile endeavour towards early detection and treatment of cancer. With increasingly robust knowledge of cancer progression at the molecular level, unique biomarkers such as kinase pathway checkpoints and over-expression of surface integrin have been identified in specific tumor cells (Henry and Hayes 2012, Goossens *et al.* 2015). Unique biomarkers can serve as target molecules for detection and drug delivery.

Discoveries in cancer-specific biomarkers have profoundly innovated nanoparticle design strategies. Tumor targeting can refer to the targeting of molecular pathways essential to tumor proliferation, vascularization, and/or metastisis. Proteins involved in pathways essential to tumor growth can be referred to as biomarkers. Inhibitors can be used to block these pathways, to reduce tumor viability and/or growth. Many of the current targeting inhibitors are protein kinase inhibitors as several key pathways that amplify tumor proliferation and metastasis are associated with protein kinase mutations and/or overexpression (McDermott and Settleman 2009, Chapman P.B. *et al.* 2011, De Mattos-Arruda *et al.* 2011, Bailey *et al.* 2014). Tumor targeting can also refer to delivery through binding specific proteins expressed on the surface of tumor cells. This strategy pairs theranostic molecules with ligands that specifically bind surface molecules overexpressed and/or unique to certain tumor cells. Table 1 depicts several cancer-specific biomarkers relevant in tumor targeting. As an example, various integrins are over-expressed in specific cancer cells and recycled to the surface at a higher rate in tumor cells compared with healthy tissue (Desgrosellier and Cheresh 2010, Ley *et al.* 2016). Naturally, integrins bind native extracellular ligands at receptor binding sites to mediate specific cellular pathways, such as internalization of integrin-bound ligands. Integrins are also involved in focal adhesion formation and cell motility, capable of promoting tumor metastasis and growth as well as pro-angiogenic and pro-tumorigenic alterations in the tumor microenvironment (Subbaram and Dipersio 2011). Consequently, integrin targeting for tumor-specific delivery as well as integrin inhibition, have been explored as cancer theranostic strategies.

In recent decades, rigorous structural and biochemical investigation in to cell-receptor binding sites has resulted in the construction of modified and/or synthetic peptides that target surface molecules overexpressed in tumor tissue, favoring those with low transient levels of expression in healthy epithelial cells (Srinivasarao *et al.* 2015). As an example, synthetic peptides have been developed to target αVβ3 integrin, which is overexpressed in many cancerous tumors including glioblastoma, prostate, pancreatic, breast and cervical. Incorporating a previously described integrin-specific RGD motif as a backbone, one-bead one-compound libraries were synthesized to discover a peptide highly specific to αVβ3 integrin (Xiao W. *et al.* 2010). This study demonstrated the specific targeting potential of the synthetic peptide to various tumor cells (known to overexpress αVβ3) both *in vitro* and in animal models. While tumor-specific synthetic ligands exhibit high specificity for targeted cancer cells, naked peptides are often susceptible degradation in physiological conditions, limiting their bioavailability. Instead of naked peptide delivery, genetic modification and/or chemical modulation strategies are used to affix peptides to the surface of nanoparticles for ligand protection against harsh physiological conditions. As a multifunctional delivery vector, a nanoparticle can simultaneously integrate theranostic molecules and tumor targeting ligands for theranostic delivery (Xu *et al.* 2015, Barwal *et al.* 2016, Luque-Michel *et al.* 2016).

TABLE 1 Example biomarkers used for tumor-specific targeting. Several protein kinases (McDermott and Settleman 2009, Bailey *et al.* 2014, Goossens *et al.* 2015) and integrins (Desgrosellier and Cheresh 2010, Ley *et al.* 2016) listed with associated cancer phenotypes.

Target	Associated Molecular Phenotype In Tumors	Targeting Strategies	Cancer Indications
HER 2	Overexpression Increased cell growth/division	Inhibition & Tumor cell targeting	Breast & gastric cancer, renal cell carcinoma
EGFR	Upreg. Tyrosine kinase Increased cell growth/proliferation	Inhibition	Pancreatic cancer
BRAF	Upreg. Serine/threonine kinase Increased cell growth/proliferation	Inhibition	Melanoma
mTOR, cancer	Upreg. Serine/threonine kinase Increased cell growth, proliferation And motility	Inhibition	Breast renal Cell carcinoma
αVβ6 (Integrin)	Overexpression Red. Patient survival	Tumor cell Targeting & Inhibition	Breast, colon, lung, Prostate, ovarian, Cervical
αVβ3 (Integrin)	Overexpression Metastasis	Tumor cell Targeting & Inhibition	Prostate, pancreatic Glioblastoma, Melanoma, breast
α4β1 (Integrin)	Overexpression Metastasis & Proliferation	Tumor cell Targeting & Inhibition	Melanoma, kidney & Osteo-sarcoma

Many nanoparticles can package drug and/or detection molecules such that a nanoparticle surface protects encapsulated theranostic molecule from degradative physiological conditions. In addition to traditional fluorescent peptides, detection agents and methods include: quantum dots and up-converting nanoparticles in fluorescence and electron microscopy, gold nanoparticles in electron microscopy and near infrared absorbance imaging, and magnetic nanoparticles such as iron oxide in magnetic resonance imaging. Gold nanocluster detection agents are described in detail in the gold nanoparticles section. Additionally, examples of well-studied cancer therapeutic agents that can benefit for nanoparticle encapsulation include: nucleic acids for gene therapy such as gene silencing and/or expression (Seow and Wood 2009, Chen L.S. *et al.* 2010), metallic nanoparticles such as iron oxide (Banobre-Lopez *et al.* 2013, Espinosa *et al.* 2016) for localized hyperthermia and gold nanoparticles for photo-thermal therapy (Chen X. *et al.* 2012, Daraee *et al.* 2016), paclitaxel which causes tubulin polymerization to disrupt cell division, and doxorubicin which inhibits cancer cell nucleic acid synthesis (Brannon-Peppas and Blanchette 2004, Barwal *et al.* 2016). Once encapsulated in tumor-targeted nanoparticles, fewer drug and detection molecules are passively absorbed by healthy tissues (Dietel *et al.* 2015, Jo *et al.* 2016). This serves to not only reduce the required dosage for effective delivery, but also protects healthy tissues from accumulation of toxic theranostic byproducts. In addition, nanoparticle constructs can be selectively tuned for optimum drug release by predictable disassembly conditions and triggers.

2.1.2 Organic nanotheranostic constructs

Most effective nanoparticle formulations are composed of lipids or polymers such as liposomes, solid lipid nanoparticles, micelles, and protein assemblies. Low toxicity excipients and ready absorption of polymers and lipids have physiological advantages over wholly inorganic delivery platforms (Miller 2013). One of the most common and clinically relevant nanoparticle subtype is lipid-based drug delivery. Lipid-based nanoparticles are spherical lipid vesicles with phospholipid bilayer structure comprised of phosphor- and sphingo-lipids often containing additional natural and synthetic components. Like native liposomal structures, lipid-based nanoparticles are soluble in the extracellular environment, can bind and enter human tissue, and transport across the cell membrane. Many lipid-based systems can be modified to encapsulate both hydrophobic and hydrophilic theranostic molecules in the lipid nanoparticle core. Through encapsulation of theranostic molecules, lipid nanoparticles can protect theranostic molecules from clearance and reduce their toxicity. Additionally, they can be surface modified to attach targeting and detection molecules.

While lipid-based nanoparticle technology has substantially advanced to clinical use, there are significant challenges with lipid nanoparticle delivery. There are many ongoing efforts to improve lipid nanoparticle clearance rates, non-specific cell uptake, heterogeneity, and stability to reduce issues with

degradation and toxicity (Charron *et al.* 2015). Generally, while lipid bilayers are considerably stable structures, drug loaded formulations can be less stable and cause non-uniform drug release. For example, lipids that form a stable crystalline lattice will not properly encapsulate theranostic molecules, such that less stable heterogeneous lipid compositions are necessary for packaging. Non-uniform drug release can result from "burst release" effect which is essentially a large early release of drug molecules, followed by a slow partial drug release. Lipid-based nanoparticles can exhibit toxicity by inducing complement activation leading to negative side-effects and hypersensitivity (Zolnik *et al.* 2010). Intratumoral uptake is not always ideal with lipid nanoparticles, but various compounds can be incorporated in to the lipid surface to enhance nanoparticle internalization in tumors (Ghaghada *et al.* 2016). To overcome some obstacles associated with lipid nanoparticles, polymeric strategies have been implemented such as the incorporation of poly ethylene glycol (PEG) and synthesis of polymeric micelles (Masuda *et al.* 2009). PEG polymers on the surface of nanoparticles can reduce uptake by the reticuloendothelial system. PEG is often used to facilitate transport of theranostic particles into cancer cells (Masuda *et al.* 2009). However, PEGylated lipid nanoparticles can still undergo accelerated blood clearance, reducing their efficacy in subcutaneous delivery (Zhao Y. *et al.* 2012). One of the most significant limitations of PEGylated lipid nanoparticles is their heterogeneity in size (Zhang J. *et al.* 2013). Heterogeneity restricts the capacity to control physiochemical properties of nanoparticles for efficient delivery.

Polymeric micelles comprise another class of theranostic delivery platforms (Li Y. *et al.* 2010). Micelles are comprised of an inner core and a hydrophilic outer shell forming a two-phase structure. Optimally sized micelles can evade opsonisation, preventing phagocytic cell uptake and sequestration. Micelle morphology and surface charge/functionalization impact efficient delivery and cytotoxicity(Knudsen *et al.* 2015). Micelles can still induce hypersensitivity, causing the immune system to activate an undesirable allergic response. Micelle size typically varies, particularly upon theranostic encapsulation. This heterogeneity hinders the capacity to predict biocompatibility, cytotoxicity, immunogenicity, and efficiency of micelle delivery platforms *in vivo.* Sufficient theranostic accumulation and penetration in tumor cells also limit micelle delivery (Hare *et al.* 2017). These general obstacles have led to investment in alternative approaches to theranostic delivery.

In its earliest stages, nanomedicine was inspired by vaccine development. Early viral vaccines involved inactivated and/or attenuated viruses and are still prevalent today (Plotkin 2005). While classic vaccine strategies are effective for vaccination against less dangerous viruses such as influenza (Wareing and Tannock 2001), there is an inevitable potential for reversion to virulent phenotypes *in vivo,* particularly for RNA viruses prone to high mutation rates. While reversion to virulence is rare, classic vaccinations against more dangerous viruses such as poliovirus and foot-and-mouth disease virus can result in devastating side effects such as poliomyelitis due to vaccine induced infection (Minor 2004). To obfuscate potential reversion to virulence, empty

virus-like particles, VLPs, have been employed as clinically effective vaccine vectors. VLPs are formed from viral structural proteins that self-assemble in to stable higher-order structures resembling the respective native virus structure, but lack the necessary viral elements for infection and propagation. VLPs are most often assembled from truncated virus structural proteins capable of self-assembly, with the chief goal to preserve inherent structural stability and immunogenic epitopes of the parent virus. Several VLP-based human vaccines have been commercialized including RECOMBIVAX HB and Gardasil to vaccinate against Hepatitis B virus (HBV) and Human papillomavirus (HPV), respectively (Zhao Q. *et al.* 2013). VLPs are effective vaccination agents, not only against the virus from which the VLP originated, but also against foreign pathogens.

VLPs can be modified to expose antigenic epitopes of foreign pathogens on the VLP surface (Niikura *et al.* 2002, Tissot *et al.* 2010, Shima *et al.* 2016). Many pathogens do not form a stable immunogenic structure that can be mimicked solely by native structural protein isolation. For example, Human Immunodeficiency Virus (HIV) forms a transmembrane protein that is insoluble and not particularly stable in its truncated form. Antigenic epitopes of HIV can instead be presented on the surface of stable VLPs that are then presented to the immune system to elicit a protective immune response(Buonaguro *et al.* 2013). Applications of VLPs in nanomedicine have extended beyond vaccination; particularly towards diagnostics and chemotherapeutics (Chen L.S. *et al.* 2010, Jobsri *et al.* 2015, Chao *et al.* 2016). Hepatitis E Virus-like particles (HEV-LPs) exhibit unique gastrointestinal stability, surface domain flexibility, and packaging potential, prompting investigation in to theranostic applications of HEV-LP vectors.

2.2 HEV Nanocapsid

2.2.1 Hepatitis E Virus origin

HEV-LPs exhibit inherent physiochemical compatibility and stability because they are derived from capsid protein of Hepatitis E Virus (HEV) (Li T.C. *et al.* 1997). Classified within the *Hepaviridae* family, HEV is a non-enveloped positive sense RNA virus with three open reading frames (ORF 1-3) (Tam *et al.* 1991). HEV causes acute hepatitis in infected humans. (Kamar *et al.* 2014). Though HEV infection is often self-limiting, there are cases of chronic hepatitis upon infection and infected pregnant women are particularly vulnerable, having an increased mortality risk (Kamar *et al.* 2014, Kamar *et al.* 2015). Predominantly affecting East and South Asia, as well as parts of Africa, HEV is spread through contaminated water supplies and food, resulting in fecal-oral transmission, with little evidence of human-to-human transmission. Therefore, HEV evolved a highly stable capsid protein protecting its transmission through water supplies and harsh proteolytic and acidic conditions of the mucosal system.

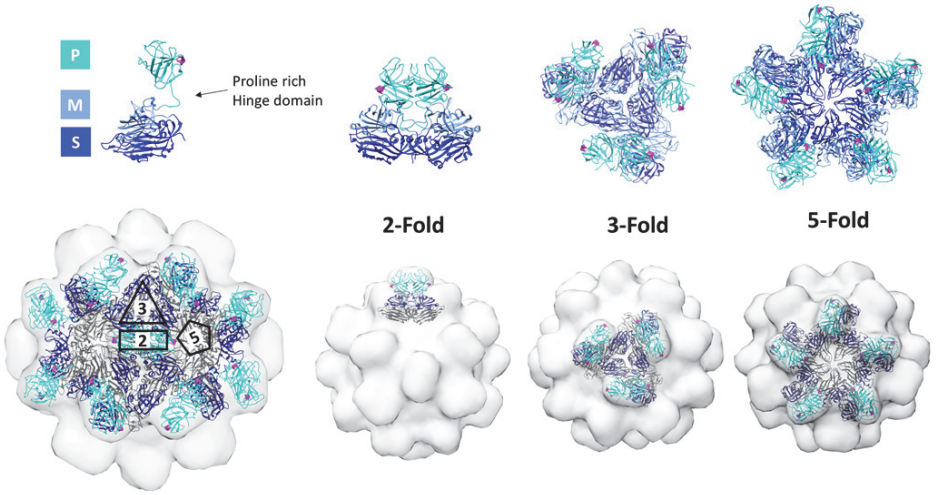

FIGURE 1 Schematic of HEV nanocapsid building blocks. S (dark blue) and M domain (medium blue) form the icosahedral base from which the P domain (cyan) extends via a flexible hinge. Nanocapsids form an icosahedral structure with a 2-fold, 3-fold, and 5-fold axis of symmetry. Subunits and surface rendered nanocapsid were generated in UCSF chimera with T=1 HEV-LP crystal structure- PDB 2ZTN (Wang C.Y. *et al.* 2008).

To provide a foundation for clinical applications, *in vitro* biochemical, structural, and cellular studies are essential. Unlike many other fecal-orally transmitted viruses such as enteroviruses, cell-culture models for HEV were inefficient and ultimately ineffective (Guu *et al.* 2009). The absence of a robust cell-culture model for HEV infection, and the lack of a closely related virus relative motivated alternative strategies to investigating HEV infection. This led to the construction of Hepatitis E virus-like particles or HEV-LPs. HEV-LPs were constructed from open reading frame 2 (ORF2) of a genotype 1 HEV sequence (Li T.C. *et al.* 1997) in various protein expression systems including bacteria, insect cell, and yeast. Some groups have produced HEV-LPs in *E. coli* by isolating the ORF2 amino acids (aa) 368-606 forming a partial HEV protrusion domain, otherwise known as p239 (Li Shao W. *et al.* 2005b). p239 is commercialized in China as a vaccine, Hecolin®, for protection against Hepatitis E infection (Li S. W. *et al.* 2015, Wu *et al.* 2016). While previous research has demonstrated that p239 structure is stable over time and can trigger protective immunity against HEV, TEM images suggest p239 structures exhibit significant heterogeneity, aggregation, and lack of high-symmetry (Yang *et al.* 2013). Hence, p239 sufficiently exposes native HEV epitopes to elicit a HEV-specific protective immune response; but, it is not ideal for specific surface modulation or packaging.

HEV-LPs produced in a Bac-to-Bac® system form homogenous, high-symmetry nanocapsids (Li T.C. *et al.* 1997, Xing *et al.* 1999, Yamashita *et al.* 2009). Bac-to-Bac® expression employs a modified baculovirus to infect insect

cells for overexpression of an inserted protein of interest. Various protein production lines are optimized and scaled up through Bac-to-Bac® expression for industrial level production (Lopez-Vidal *et al.* 2015). Several clinically approved vaccines and therapies are based on baculovirus expression technology including Cervavix® and FluBlok® (van Oers *et al.* 2015). Many proteins produced in the Bac-to-Bac® system are susceptible to cellular protease degradation such that protein recovery needs to occur several days post infection. While baculoviruses are not "lytic" viruses, the cytotoxic, high-stress environment induced by high MOI infection and protein overexpression does induce insect cell apoptosis in late expression, releasing proteins in to the extracellular environment (Gomez-Sebastian *et al.* 2014). Active protease and ubiquitin/proteasomes are also released upon apoptosis, often resulting in degradation of proteins of interest. Nanocapsids, however, are highly resistant to the degradative conditions of ruptured cells and do not need to be recovered at earlier stages of infection. Self-assembled HEV nanocapsids are collected 6-7 days post infection to maximize protein production (Xing *et al.* 2010). Late expression not only maximizes nanocapsid production, but also, the apoptotic release of nanocapsid from insect cells eliminates cell lysis/purification steps.

HEV nanocapsids are composed of ORF2 aa 112-606 that assemble in to a (S-) and membrane (M-) domain icosahedral base that stabilizes a surface exposed protrusion (P-) domain through a flexible proline-rich hinge (Guu *et al.* 2009, Xing *et al.* 2011). While p239 forms a cluster of dimers stabilized by P-domain interactions, nanocapsid dimers are additionally stabilized by 3- and 5-fold interactions between the S- and M-domains (Fig. 1). Native HEV capsid protein assembles 180 symmetric repeated units, having T=3 symmetry. T=3 symmetry indicates the icosahedral structure is composed of 12 pentameric and 20 hexameric capsomeres comprising a total of 180 subunits. HEV nanocapsids are empty nanocapsids with T=1 symmetry composed of 52 kDa monomeric subunits. T=1 symmetry means 12 pentameric capsomeres form the icosohedral capsid from 60 subunits. Previously, HEV-LPs produced without a 112 amino acid truncation at the N-terminus exhibited T=3 symmetry (Xing *et al.* 2010). HEV-LPs with T=3 symmetry resembled native HEV in EM but, unlike T=1 nanocapsids, T=3 HEV-LPs could not disassemble and reassemble *in vitro.* Whereas nanocapsids are empty, T=3 HEV-LPs retained encapsulated RNA, which is thought to be required for HEV T=3 assembly. In addition to reversible assembly *in vitro*, T=1 nanocapsids have a more prominent spike-like P-domain than both T=3 HEV-LPs and native HEV, increasing surface exposure of the P-domain (Fig. 2).

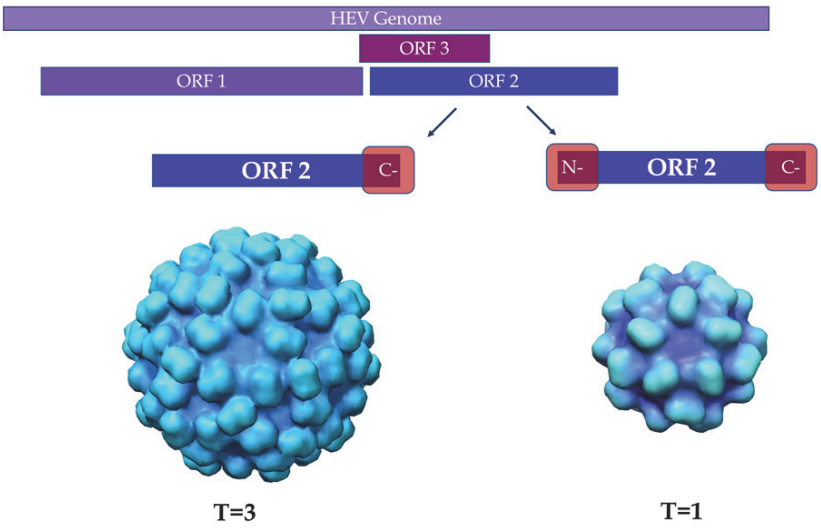

FIGURE 2 T=3 and T=1 nanocapsid assembly. Full-length N-terminal HEV-VLPs self-assembles with 180 identical subunits and is approximately 40 nm in diameter. N-terminal truncation results in a T=1 nanocapsid formation from 60 identical subunits measuring about 27 nm in diameter. T=3 nanocapsid packages RNA while T=1 does not. T=3 nanocapsid was generated in UCSF Chimera with PDB 3IYO (Xing *et al.* 2010).

2.2.2 Mucosal stability and *in vitro* packaging

Oral delivery is often the desirable alternative to parenteral administration in diagnostic and therapeutic delivery. From a broad perspective, oral delivery is not only cheaper than subcutaneous delivery, but is also more accessible to individuals in developing countries where trained medical professionals and a regular supply of sterile needles are not easy to come by. For cancer treatment specifically, oral alternatives to injection benefits patient comfort and continuous cancer cell exposure to therapeutics, particularly in the case of chronic treatment. Continuous exposure to a chemotherapeutic also allows for a lower, less toxic drug dosage. Most theranostic molecules and many nanoparticle vectors are unstable in the mucosal system due to harsh gastrointestinal (GI) conditions such as severe pH fluctuations, digestive enzymes, microfluora, and rapid GI emptying. (Thanki *et al.* 2013, Date *et al.* 2016). Perhaps the most obvious advantage of HEV nanocapsid delivery vectors is their mucosal stability. Inherent in their evolutionary origin as feco-orally transmitted viruses, nanocapsids are well suited to normally degradative, low pH and proteolytic conditions. Nanocapsids are highly stable in storage conditions as they can withstand high temperatures and last years in 4°C. As previously mentioned, HEV human-to-human transmission is uncommon; rather, most virus is transmitted through a contaminated water supply. With no apparent water-born host, this suggests that HEV remains stable in the various harsh conditions of sewage and other contaminated water supplies.

Furthermore, HEV is prevalent in South and East Asian countries, many of which are renowned for +40°C summer days. This stability is invaluable considering the exorbitant shipping and storage costs and limitations associated with temperature and time sensitive therapeutics.

Nanocapsids can encapsulate theranostic molecules through reversible Ca^{2+} mediated assembly. A N-terminal truncation in ORF2 encoding the nanocapsid protein prevents assembling nanocapsids from encapsulating genomic RNA during production (Xing *et al.* 2010). Internal residues facing the empty nanocapsid cavity can still participate in ionic interactions to package and protect theranostic molecules. This protection can serve to either control theranostic release and increase absorption, or to target specific GI tissues. Nanocapsids can package negatively and neutrally charged molecules, particularly nucleic acids, through *in vitro* Ca^{2+} mediated disassembly and reassembly. Nanocapsids are disassembled in to dimer subunits through chelation with one of two chelating agents, ethylenediaminetetraacetic acid (EDTA) or ethylene glyco-bis(β-aminoethyl ether)-N ,N ,N ´N ´-tetraacetic acid (EGTA) in reducing conditions with dithiothreitol (DTT). Negatively charged molecules, such as nucleic acids, are added to the disassembled nanocapsids for ionic interaction with positively charged nanocapsid residues that line the interior surface of the assembled nanocapsid cavity. Subsequent dialysis in a Ca^{2+} rich buffer to simultaneously remove reducing and chelating agents and add Ca^{2+} ions, triggers capsid reassembly. During reassembly, nucleic acids or negatively charged molecules will remain ionically associated with the interior nanocapsid residues, resulting in encapsulation of these molecules.

Previously, Ca^{2+} mediated nanocapsid encapsulation was employed to package foreign DNA for applications in gene therapy and vaccination (Takamura *et al.* 2004). In the first set of experiments, various sized plasmids, ranging from 3-11 kB were packaged in VLPs and assessed for encapsulation efficiency. Plasmids within this size range were successfully encapsulated but reduced packaging efficiency was observed as the plasmid size increased. After confirmation of foreign DNA expression in cells using a nanocapsid transfection agent, several immunological studies were carried out. A plasmid encoding HIV envelope protein gp120, or HIV-env, was encapsulated in nanocapsid for oral and subcutaneous delivery in mice. Naked HIV-env plasmids and empty nanocapsids served as negative controls. From subcutaneous delivery, HIV-env specific IgG was detected in sera but not IgA. Following oral administration, HIV-specific IgG was detected in sera and HIV-specific IgA was detected in fecal extracts. These results suggested oral administration of HIV-env plasmid DNA encapsulated in naocapsids elicited a humoral response. Additionally, oral administration resulted in HIV-specific cytotoxic T lymphocytes at local mucosal sites and systemically. However, as expected, HEV-specific IgG and IgA were detected in sera and fecal extracts, particularly following oral delivery.

This study makes a strong case for successful oral gene delivery via nanocapsid encapsulation, particularly with the goal of eliciting an immunological response. However, this study also highlights some of the

limitations of nanocapsids that have also been well documented in other viral-vectors for gene delivery. First, the DNA packaging limitations should be considered. While the study suggested up to 11 kB plasmids could be packaged, packaging efficiency substantially decreased as a function of plasmid size; hence, a smaller plasmid was encapsulated for immunological studies. Another important feature of nanocapsids is their high immunogenicity. While excellent for vaccine design, the elicitation of an innate and adaptive immune response can be problematic for bioavailability, particularly in the case of repeated administration (Hasbrouck and High 2008, Zolnik *et al.* 2010). Some of these issues can be avoided with interchangeable surface modulation techniques.

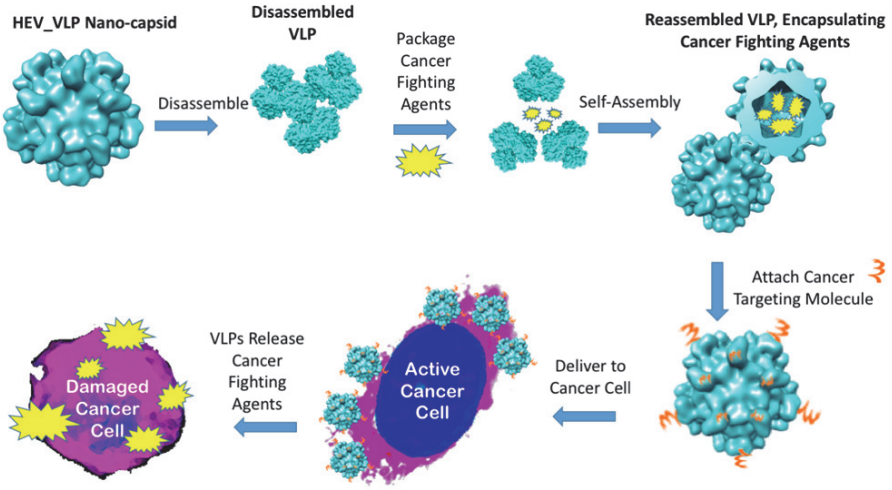

FIGURE 3 Schematic of nanocapsid surface conjugation, theranostic encapsulation, and cancer cell delivery.

2.2.3 Nanocapsid surface modification and modulation

Because the spike-like P-domain that extends away from the icosahedral base through a flexible hinge, P-domain modification has limited impact on the capsid structure. Early nanocapsid research demonstrated foreign peptide insertion in to the nanocapsid C-terminus resulted in sufficient exposure of the peptide *in vivo* without altering the nanocapsid assembly (Li T.C. *et al.* 1997). In subsequent studies, six nanocapsid sites were tested for foreign epitope insertion, demonstrating successful foreign epitope exposure, stability, and immune recognition upon oral administration (Niikura *et al.* 2002). More recently, HIV epitope p18, was inserted in to the top-most surface of the P-domain dimer at aa 485 in ORF2 (Jariyapong *et al.* 2013, Cheng R. Holland and Xing 2014). Though icosahedral nanocapsid indeed formed following p18 insertion, SDS-PAGE results displayed a 42 kDa band instead of the expected 52

kDa band. Further investigation showed that a trypsin cleavage site was introduced upon p18 insertion at Y485 resulted in cleavage of the remaining 486-606 aa residues. To test the effect of trypsin, protease inhibitors were introduced during protein production and purification. Recombinant nanocapsids with p18 insert generated in the presence of protease inhibitors also formed icosahedral nanocapsids, but showed 52 kDa monomeric bands. Hence, substantial C-terminal truncation (486-606) did not deter icosahedral capsid assembly. Additional experiments were carried out to determine whether the nanocapsid with p18 insert would be susceptible to trypsin cleavage in its assembled state. Following the removal of protease inhibitor, assembled and disassembled nanocapsids were separately treated with trypsin, and run through SDS-PAGE. Assembled nanocapsids were not trypsinized, retaining 52 kDa banding, whereas disassembled nanocapsids showed 42 kDa banding. The p18 peptide was intentionally inserted in to a highly solvent-exposed epitope on the nanocapsid, such that the trypsin cleavage site was also highly exposed. However, assembled nanocapsid sufficiently protected this exposed insert from protease cleavage. These combined oral delivery and protease resistance studies highlighted the nanocapsid resistance to proteolytic environments and its stabilization of surface-exposed epitopes.

Genetic insertion is not ideal in all cases of modification, given the time required to genetically engineer a new construct and limitation to naturally occurring amino acids. Conversely, chemical bioconjugation is an efficient method to affix naturally occurring and synthetic peptides to a biomolecular surface. In organic chemistry, conjugation is the aligned overlap of p-orbitals, alternating single and double bonds, resulting in electron delocalization. Chemical conjugation of biological constructs, also referred to as bioconjugation, can generate multifaceted functionalization strategies in theranostic development (Stephanopoulos and Francis 2011). Unlike antibody binding strategies, bioconjugation can irreversibly bind theranostic molecules to a biological construct. Bioconjugation is typically a reaction between a small molecule, such as a peptide or organically linked molecule, and specific residues on a biological platform. Unlike classic organic chemistry reactions with small molecules, the design of bioconjugation reactions must take in to account both optimal chemical reactivity conditions and biological structure to ensure conjugation efficiency and biological compatibility. For example, lysine conjugation is one of the most prevalent bioconjugation reactions through N-hydroxysuccimide (NHS) coupling with the primary amine group on lysine. It is also useful to note that NHS-lysine conjugation requires alkaline buffer conditions, which can destabilize some biological constructs (Basle *et al.* 2010). Because lysine is a hydrophilic residue, there are typically multiple lysine sites on a protein surface, such that lysine conjugation is relatively efficient for non-specific labelling with detection reagents such as fluorescent probes. However, with multiple native lysine residues available for binding, it is difficult to carry out site-specific conjugation. Site-specific conjugation is essential to finely tuned surface chemistry. It is preferable to have non-native engineered binding sites to more accurately control bioconjugation reactions.

Site-directed cysteine conjugation has proved to be one of the most effective techniques to covalently bind biological constructs. Cysteine conjugation is carried out through the nucleophilic sulfhydryl side chain (thiol group) of cysteine. Example cysteine conjugates include: maleimide and maleimide derivatives, allenamides, 2-cyanobenzothiazone, derivatives of phenyloxadiazole, and thiol-protection groups (Bernardes *et al.* 2008, Chalker *et al.* 2009, Cal *et al.* 2014). Thiol reactions are amenable to biological construct stability because conjugation can be achieved in low temperatures at neutral pH *(6.5-7.5*). Conveniently, nanocapsids do not express a native surface-accessible cysteine, such that an engineered cysteine would be the only exposed binding site for thiol conjugation. A schematic of nanocapsid delivery combining conjugation and packaging of cancer theranostics is depicted in Fig. 3.

2.3 Gold nanoparticles in biology

2.3.1 Classic gold nanoparticles and applications

Gold nanoparticles (AuNPs) are widely used to image biological samples by distinguishing the unique light and electron absorption properties of AuNPs from biological carbon-based molecules. Unlike many other heavy metal nanoparticles, AuNPs exhibit low toxicity, minimal oxygen sensitivity, and are relatively inert (Ackerson *et al.* 2010a, Daraee *et al.* 2016). The surface chemistry of various AuNPs is well understood following decades of research, with many available protocols for AuNP synthesis as well as commercially available constructs. Three biological applications of AuNPs include: 1.) electron microscopy, where the high electron density of AuNPs is distinguished from biological material; 2.) near-infrared imaging, exploiting the size and shape-dependent localized surface plasmon resonance of AuNPs; and 3.) NIR absorbance induced photothermal effect of AuNPs.

Perhaps the predominant biological application of AuNPs is in electron microscopy (EM). With an electron dense core, AuNPs serve as contrast agents for image alignment, single particle reconstruction, immunolabeling, and direct biomolecule tracking. In these EM applications, the high electron density of AuNPs generates high phase and amplitude contrast close to focus, distinguishing them from biological compounds, comprised of lower density organic material. AuNPs can be used as markers to align tomography images in a tilt series or to align a stack of imaged tissue sections through 3D serial reconstruction. AuNPs can participate in non-specific electrostatic interactions with biomolecules such as nucleic acids, but such interactions are typically only identifiable in an isolated system. AuNPs can label thiolate-functionalized oligonucleotides to bind specific DNA sequences, with additional steps to reduce non-specific electrostatic interactions between AuNPs and DNA (Ackerson *et al.* 2005, Ackerson *et al.* 2010b). One of the most widely used AuNP applications is immunolabeling (Sperling *et al.* 2008, Powell and Hainfeld 2011).

AuNP-conjugated secondary antibodies are commercially available to secondarily label antibody-bound biomolecules of interest. For primary immunolabeling, AuNPs can be conjugated directly to a primary antibody or antibody fragments that bind a protein of interest in a thin layer of vitreous ice or in an embedded cell sample (Griffiths and Lucocq 2014, Yi *et al.* 2015). Colloidal AuNP conjugation is also used for *in situ* immunolabeling of pre-embedded samples to enhance epitope accessibility. This method often requires some form of cell permeabilization which can damage cell-structure (Orlov *et al.* 2015). Antibodies labeled with AuNPs can be bound to viruses for macropinocytotic cell-entry (Rintanen *et al.* 2012); however, antibody binding is a reversible, non-covalent interaction, such that background signal and antibody degradation can impact results. AuNP immunolabeling is particularly useful for imaging low-contrast cryoEM samples to identify specific biological structures.

CryoEM offers a unique window in to biological interactions at the nanoscale because native structure and interaction are instantly "locked in time" through cryogenic preservation. Other methods of sample preparation, such as chemical fixation or negative staining, tend to introduce artifacts and structural damage, resulting in a less accurate depiction of a biological construct. In cryoEM, samples are rapidly preserved in a thin vitreous layer of ice and imaged at cryogenic temperatures. The high energy of electrons causes slight movement or sample "drift" and eventually melts the vitreous ice; during which time, electron irradiation damages and alters biological structure (Shigematsu and Sigworth 2013, Guo and Jiang 2014). Low electron dosage imaging partially accommodates the biological and temperature sensitivities, but this vastly reduces the phase contrast of cryoEM images. Historically, these limitations dwarfed cryoEM resolution compared to the atomic resolution attained by X-ray crystallography. Because X-ray crystallography samples are tightly packed into crystals, X-ray samples have a much higher radiation tolerance and more molecules typically contribute to a single diffraction. However, crystal packing leads to loss of variable and heterogeneous protein features and interactions because structures that cannot be crystalized, such as asymmetric constructs, cannot be imaged in X-ray crystallography. Not only can heterogenous features be observed in cryoEM, but also, the achievable resolution of cryoEM has vastly improved in the past five years (Cheng Y. 2015, Frank 2017). A key hallmark in cryoEM advancement was the recent introduction of direct electron detection devices (DDDs). In addition to improving image quality with direct electron detection, DDDs have sufficient image acquisition rates to track sample "drift" through a series of images in a single exposure. A DDD image series from a single exposure is then analyzed both manually and through motion correction software to produce images with resolution unachievable by the predecessor CCD cameras (Bai *et al.* 2013, Bai *et al.* 2015). Other substantial improvements include semi-automated sample preparation and loading, automated image acquisition, phase plate technology, 3D reconstruction software developments, and optimized detection agents. These combined innovations are pushing cryoEM structure determination to

atomic resolution. Following this trend in high-resolution cryoEM, detection agent size and uniformity are imperative.

Many of the AuNP constructs referenced in the literature are colloidal gold particles. Currently, most AuNPs used in biological applications have an organic polymer surface that helps to control the size, charge, and aggregation of the AuNP. AuNPs can be synthesized and purified in various sizes and charge, both of which determine their optical properties (Daniel and Astruc 2004). In addition to ionic interactions with biological material, the AuNP surface can be functionalized for conjugation and/or targeting purposes. For image alignment and protein localization, the size range of colloidal gold (typically between 5-50 nm) is effective (Daraee *et al.* 2016). However, to detect domain specific structure and interactions at a nanoscale, even the smallest colloidal gold particles are relatively large at high resolution. Some smaller gold colloids have been developed but they are not often monodisersed. Colloidal gold is sometimes described as monodispersed, but colloidal gold particles tend to exhibit size heterogeneity in solution with anywhere from 5-15% size variation (Ackerson *et al.* 2010a). This size heterogeneity is attributed to the various crystal structures that comprise a single colloidal gold population. Advancements in cryoEM technology has driven structure investigation to angstrom scale distances, where colloidal gold is no longer sufficiently small or structured for high-resolution detection.

2.3.2 Molecule-like monolayer protected gold nanoclusters

A new class of gold nanoparticles are prepared as discrete small clusters of gold atoms protected by a surface monolayer, henceforth referred to as monolayer protected gold nanoclusters (AuNCs). Unlike colloidal gold nanoparticles, AuNCs form a substantially smaller gold core (0.5–2 nm) and have a uniform crystal structure. The hydrophilicity and symmetric orientation of the protective monolayer readily solubilize AuNCs in water. From these uniform characteristics of AuNCs emerge molecule-like qualities where AuNCs monodisperse in solution with limited atomic size variability (Salorinne *et al.* 2014, Azubel and Kornberg 2016). The small size and structural consistency of AuNCs are ideal for labeling biomolecules.

Despite the small size of AuNCs, the electron rich core of AuNCs is distinguishable from organic material in EM imaging. As detection labels, the small size of AuNCs allows for more precise position localization of an associated biological structure or interaction. Furthermore, biocompatibility of AuNCs can be better controlled than that of colloidal gold particles because of AuNC uniformity. Previous toxicity studies have shown that variation in gold nanoparticle size and charge can affect cytotoxicity (Albanese *et al.* 2012). In addition to charge, the length of surface protection ligands can impact cell circulation and uptake (Kang *et al.* 2015). Size consistency and symmetric monolayer distribution aid in predicting and assessing interactions between gold surface ligands and biomolecules. Hence, the uniform crystal structure of

AuNCs is preferred over colloidal gold for biological applications (Koivisto *et al.* 2016).

AuNC structure and size are highly interdependent, such that even a single atom change can dramatically alter the intrinsic AuNC properties. AuNC crystal structure stability emerges from the "magic number" principle, where clusters composed of a specific number of gold atoms are magnitudes more stable than clusters formed from gold atomic numbers between and outside of those "magic numbers." Consequently, AuNCs are synthesized with atomic precision. Often, AuNCs have a thiolate protective monolayer $Au_n(SR)_m$ such as *p*-mercaptobenzoic acid or $Au_n(p\text{MBA})_m$, and more recently $Au_n(3\text{-MBA})_m$ (Azubel and Kornberg 2016). The thiolate monolayer maintains an atomically homogenous, water soluble AuNC population. Soon after describing the formula for magic thiolate-protective clusters, $Au_n(SR)_m$ (Negishi *et al.* 2005), a mechanism of gold cluster protection by Au-thiolate oligomers (Hakkinen *et al.* 2006) and the first crystal structure of a thiolate protected cluster, $Au_{102}(p\text{MBA})_{44}$ (Kornberg, 2007) were determined. These achievements led experts in chemistry and structural biology to meet at the forefront of investigating biological applications of thiolate-protected AuNCs.

A well described thiolate-protected cluster, $Au_{144}p\text{MBA}_{60}$ (Au_{144}) was previously used in EM imaging for biomolecule detection (Ackerson *et al.* 2005). Surface ligands of Au_{144} can participate in Murray place exchange reactions, also known as ligand exchange reactions, where surface thiolate is replaced with another thiolate ligand. In this way, biomolecules containing a solvent exposed thiol replace a single *p*MBA ligand, directly conjugating biomolecules to the gold-thiolate interface. Au_{144} has been used to conjugate DNA oligonucleotides for DNA labelling (Ackerson *et al.* 2005) and single chain variable fragments (scFv) for protein labelling (Ackerson *et al.* 2006, Ackerson *et al.* 2010b) through direct ligand exchange. In contrast to AuNC conjugation, colloidal AuNP immunolabeling limits resolution because of the larger size and heterogeneity of colloidal AuNPs. In addition, to achieve covalent interactions, colloidal AuNP conjugation requires an extended functionalized linker, further distancing conjugate biomolecules from the colloidal gold density. With ligand exchange reactions, AuNCs can be directly conjugated to scFv, reducing the distance between the scFv binding site and the high density AuNC core. Gold immunolabeling is often used to track or identify specific biological structures or interactions in CryoEM or FIB/SEM. Even with direct immunolabeling, the AuNC binding site is not in direct contact with the protein of interest. In addition, problems with permeability, antibody degradation, and non-covalent antigen binding are still relevant to AuNC-bound antibody fragments. Alternatively, biological constructs of interest can be engineered with an exposed thiolate to directly bind AuNCs.

Colloidal gold conjugation to cysteine-engineered cowpea mosaic virus (CPMV) was one of the earlier examples of gold conjugation to large symmetric complexes (Wang Q. *et al.* 2002). Cysteine sites were inserted in to the CPMV surface to bind maleimde-functionalized colloidal AuNPs. In these studies, cysteine-containing peptides were inserted to form an exposed loop. Initial

cysteine replacement of surface-exposed CPMV residues resulted in irreversible aggregation such that cysteine modification in highly solvent exposed domains required well-maintained reducing environment (Wang Q. *et al.* 2002). Given the problems with maintaining a reducing environment in a biological context, cysteine loops were inserted in less solvent accessible domains to avoid disulfide-binding between cysteines. The introduction of cys-loops as opposed to single site cysteine mutation likely increased the probability of aggregation. Follow-up studies of single site cysteine replacement suggested CPMV constructs mutated with a solvent exposed cysteine were also prone to aggregation (Steinmetz *et al.* 2007). With these design decisions in mind, Nanogold® (Nanoprobes Inc.) conjugation to CPMV cysteines was successful using linker functionalized Monomaleimido Nanogold®. Monomaleimido Nanogold is a 5 nm colloidal AuNP, occupying approximately 17% of the total virus diameter. Later, 3D reconstruction and difference mapping depicted gold densities on the CPMV surface (Blum *et al.* 2004). The size of these AuNPs, in addition to the heterogeneity, left much to be desired in terms of achievable resolution. Nevertheless, this was groundbreaking work for its time, and provided a foundation for future AuNP conjugation to symmetric capsid surfaces.

In the earliest example of AuNC conjugation to virus, AuNCs were functionalized with a maleimide linker to conjugate native enterovirus (EV) cysteines (Marjomaki *et al.* 2014). In this study, a 1.5 nm AuNC, $Au_{102}(pMBA)_{44}$ (Au_{102}) was functionalized with N-(6-hydroxyhexyl)maleimide ($Au_{102}C_6MI$) to access native cysteines just below the EV surface. Two enteroviruses, Echovirus 1 (EV1) and Coxsackievirus B3 (CVB3), were successfully bound to $Au_{102}C_6MI$ through maleimide-thiol conjugation, validated by EM imaging. *In vitro* tests post-conjugation suggested virus infectivity was unaffected and perhaps even slightly enhanced by AuNC conjugation. It was necessary to carry out conjugation for two days at 37˚C to observe significant gold binding, after which EV1 and CVB3 capsids appeared to undergo some structural changes. To reduce conjugation time, temperature, and structural changes, these experiments could be further optimized with engineered, solvent-exposed cysteine sites.

To optimize surface modulation and packaging techniques, it is beneficial to first understand native virus-host cell interactions such as cell entry, gene expression and nucleic acid packaging. As previously mentioned, HEV does not have an efficient cell model to study native cell trafficking. Enteroviruses, on the other hand, have excellent cell models. Much accumulated data on enterovirus infection has provided key insights, not only in to enterovirus disease pathogenesis, but also in to fundamental virus-host-cell interactions that trigger key trafficking events such as receptor binding, cell-entry, genome release, expression, and genome packaging. While current infectious viral vectors are largely avoided as theranostic gene delivery tools, elucidating critical mechanisms of enterovirus infection efficiency can offer an invaluable perspective on nanotheranostic vector design.

2.4 Enterovirus delivery

Enterovirus (EVs), especially viruses belonging to group B subspecies (EVBs; Echoviruses, Coxsackie B viruses, and Coxsackievirus A9), are responsible for global human infections resulting in illnesses varying from mild gastrointestinal and respiratory symptoms to severe conditions such as myocarditis, meningitis, Type I diabetes, and flaccid paralysis. EVs, classified in the Picorniavirus family are non-enveloped single stranded positive-sense RNA viruses with capsid proteins VP1-VP4 encoded in the P1 region, and non-structural proteins encoded in the P2 and P3 regions. Structural EV proteins, particularly VP1, has previously been used to trace the evolution of Picornaviruses (Oberste *et al.* 1999b, Oberste *et al.* 1999a). While their capsid proteins (P1) share type-specific homology, EVB non-strucutral proteins (P2 and P3) appear to be homologous in terms of species but not in type. Given the disparity in homology between non-structural and structural virus proteins, it has been suggested that these two regions have evolved separately, potentially due to well-established independent functions of these regions in virus replication (Simmonds 2006). Moreover, high mutation rate and recombination serve adaptive purposes in tissue tropism (Muehlenbachs *et al.* 2015). EVB recombination has been previously reported in nature, further supporting EVB recombination as an adaptive function (Bouslama *et al.* 2007).

Despite binding different cell surface receptor types, EVBs are comparable in structure, exhibiting remarkable similarities in the pathways they elicit and infection kinetics (Marjomaki *et al.* 2015). EVBs normally lyse cells during infection, but especially in target tissues, many EVB subspecies appear to undergo persistent infection. The viral mechanisms responsible for these differences have not been characterized. This information is important to understand the mechanisms of infection in the target tissue.

Some Coxsackie B viruses (CVBs), such as CVB2 and CVB5 exhibit persistent non-lytic infection even within specific cell culture types, such as Rhabdomyosarcoma (RD) cells and lytic infection in others, such as HeLa cells. Persistent infection in RD cells is attributed to the low transient expression of host-cell receptor, Coxsackie Adeno-Associated Receptor (CAR). Previous studies with CVB2 suggested that serial passaging of CVB2 in RD cells resulted in an adaptation to lytic infection phenotype (Gullberg *et al.* 2010b). This adaptation was attributed to a single residue mutation on the VP1 capsid protein. Previously, distinctions in infection phenotype have been attributed to cell receptor binding. Cytolytic adaptation following serial RD cell passaging have been reported for CVB3 infection as well (Zautner *et al.* 2006, Carson *et al.* 2011). In addition, 5′ deletion in CVBs is associated with persistent infection (Chapman N.M. *et al.* 2008).

Previously, a plasmid cassette encoding the non-structural proteins (NSPs) of CVB5 was used as a backbone to exchange structural proteins (SPs) of similar EVB subspecies. Just as CVB5 binds cell receptors CAR and Decay

Accelerating Factor (DAF), the SPs recombined in the plasmid cassette were derived from EVBs that bound CAR and/or DAF as well (Jonsson Nina *et al.* 2015a). Infectivity of these chimeric viruses was comparable to that of parent enterovirus B subspecies. Recombination between CVB5 and an EVB subspecies that does not share one or both of CVB5's cell receptors has not been shown.

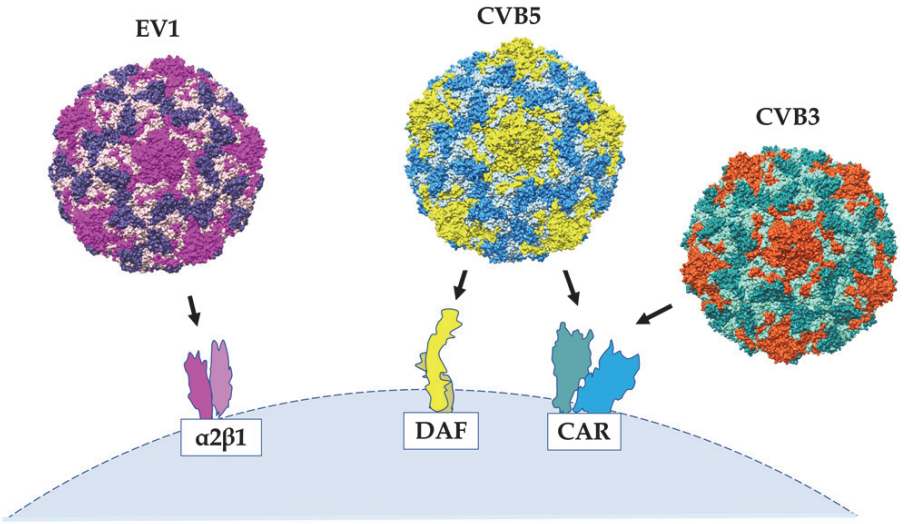

FIGURE 4: Differential receptor binding of EVBs. EV1 host-cell entry is mediated by α2β1 integrin receptor binding while. CVB5 binds both DAF and CAR host-cell receptors while CVB3 only binds CAR.

Identifying specific proteins involved in native EVB delivery is informative for theranostic delivery. Fig. 4 depicts the cell-receptors for three different EVBs. Though often not immediately realized, EVB studies can coincide with, and even lead to cancer cell biology insights. To highlight just how quickly the intersection is met between EVB delivery and cancer molecular biology, one can look to fundamental EVB subspecies Echovirus 1 (EV1). EV1 binds host-cells through a collagen cell-receptor, α2β1 integrin, inducing integrin clustering and virus internalization through macropinocytosis (Bergelson *et al.* 1993, Upla *et al.* 2004). A team studying virus-integrin interactions, determined that unlike collagen, EV1 bound the inactivated, or closed, α2β1 integrin form (Jokinen *et al.* 2010). The dogma of α2β1 conformational signaling suggested integrin clustering required integrin activation, or extension. Given that EV1 both bound the closed conformation and triggered integrin clustering, these findings contributed to an undercurrent of data suggesting there was much more to be discovered regarding conformational integrin signally. Conformation-specific integrin interactions, including those of α2β1 (Zeltz *et al.* 2010, Santio *et al.* 2016), are closely tied to cancer biology as many cancer-cells overexpress integrin unique to that tumor subtype.

2.5 Summary of review

In the field of nanotheranostics, nanoparticles are engineered to improved tumor targeting, tumor detection, bioavailability, and stability with the intention to achieve early and accurate diagnosis and effective theranostic delivery. Many detection and therapeutic agents are not stable in systemic circulation, limiting effective tumor uptake. Without specific tumor delivery, tumors cannot be fully removed without substantially damaging healthy tissues. These obstacles can be overcome with tumor-targeted nanotheranostics.

Hepatitis E nanocapsids have promising qualities of mucosal stability, surface flexibility for modulation, and the capacity to encapsulate nanoparticles *in vitro*. Previous vaccine and gene therapy studies with recombinant HEV nanocapsids have validated the mucosal stability and delivery potential of nanocapsids in both subcutaneous and mucosal administration. These qualities may be beneficial in cancer theranostic delivery as well. Nanocapsids have been previously shown to protect peptides recombined on the nanocapsid surface and nucleic acids encapsulated in the nanocapsid cavity. Moreover, nanocapsids can expose peptides for cell recognition, as well as deliver DNA for gene expression. The surface flexibility of nanocapsids suggests their capacity for significant chemical modulation with detection and tumor-targeting agents as previously depicted (Fig. 3).

Gold nanoparticles are well-described theranostic agents with biomedical applications. The monodispersed AuNC is a more recent innovation in gold nanoparticle technology, distinct from that of classical colloidal gold and Nanogold® particles. AuNCs form a single crystal structure in solid phase, are homogenous in solution, and can covalently bind biological constructs via cysteine conjugation. The molecule-like qualities and high electron density of AuNCs is critical for to achieve high resolution biological structure determination and detection in cryo EM.

Aspects of effective cell-receptor targeting for cell binding and internalization can be better understood with native enterovirus vectors. Host-cell receptors such as integrin are highly relevant in tumor-targeting both as antigen targets and tumor binding targets. The subsequent steps following receptor binding are critical to effective theranostic internalization and/or theranostic release in tumor cells. Viruses are master cell-delivery agents, such that they have evolved to bind receptor targets following specific receptor-mediated entry and/or gene release. While native HEV has neither a sufficient cell culture model nor a known host-cell receptor, EVBs are widely studied in cell culture and have defined host-cell receptors. Better understanding host-cell receptor mediated entry as well as replication and expression kinetics can provide insight in to host-cell surface targeting strategies for effective delivery of theranostic particles.

3 AIMS OF THESIS

The aims of this thesis were:

A Engineer HEV nanocapsids with a single, solvent-exposed cysteine for conjugation optimization and characterization (I, III).

B Demonstrate tumor-specific binding, internalization, and detection in cells and animal models with tumor-targeted HEV nanaocapsids, (I).

C Characterize nanocapsid conjugation to monodispersed gold nanocluster via direct place exchange and maleimide-thiol coupling (III) and determine the 3D structure of gold nanocluster-bound nanocapsids (III).

D Produce infectious recombinant enterovirus vector (EVCV) combining structural proteins from EV1 with non-structural proteins from CVB5 in order to compare capsid assembly, infectivity, replication, infection kinetics and infection phenotype between EVCV, parent viruses, and CVB3 (IV)

4 OVERVIEW OF METHODS

Table 2: Summary of studies used to carry out the primary research published in the thesis. Detailed methods can be found in the corresponding references, denoted as Roman numerals.

Method	Publication
Plasmid construction and amplification	I, IV
Insect cell culture	I, III
Mammalian cell culture	I, III, IV
Bacteria cell culture	I, III, IV
BactoBac HEV nanocapsid production	I, III
Enterovirus production	IV
Transfection	I, III, IV
Nanocapsid production and purification	I, III
Transmission electron microscopy (EM)	I, III, IV
CryoEM preparation and imaging	I, III
Single particle reconstruction	I, III
Immunofluorescent labelling and confocal imaging	I, IV
Western Blot & ELISA	I
SDS-PAGE/Native PAGE	I, III, IV
Conjugation	I, III
Fluorescent intensity quantitation	IV
Occupancy calculation	III
Precipitation studies	III
Gold nanocluster synthesis	III
Cytopathic effect assays	IV
Mouse xenograft studies	I
FACs	I

5 RESULTS AND DISCUSSION

5.1 Tumor-targeted nanocapsids

5.1.1 Five nanocapsids modified with a single cysteine binding site

Based on the known crystal structure and 3D reconstruction of HEV nanocapsid (Wang C.Y. *et al.* 2008, Yamashita *et al.* 2009), general biochemical principles were applied to select optimal thiol conjugation sites. Cysteine replacement was limited to solvent-exposed regions on the nanocapsid Protrusion domain (P domain). As is evident in its name, the P domain protrudes from the icosahedral base, rendering it the most accessible domain for conjugation. Importantly, the P-domain has proven to remain stable following substantial genetic modification and post-translational cleavage, suggesting a single-site replacement and modulation would be inconsequential to capsid assembly. To further preserve the capsid secondary structure, amino acids within variable loops, as opposed to beta sheets and alpha helices, were selected. The P domain engages in a critical quaternary interaction at the nanocapsid 2-fold center or dimer interface, so sites adjacent to or participating in this dimer interface were not selected for cysteine replacement. Generally, most of the selected amino acids were similar in size and charge to cysteine.

The following five residues on the nanocapsid P-domain were selected for single cysteine replacement: Y485C, -T489C, -S533C, -N573C and -T586C (Fig. 5). Residues engaged in antibody binding, cell-binding, and immune recognition, are implicitly solvent exposed for binding interactions. Accordingly, previous research describing these binding sites on HEV nanocapsids provided strong selection criteria for five candidate cysteine replacement sites (Li T.C. *et al.* 1997, Niikura *et al.* 2002, Li S.-W. *et al.* 2005a, Li Shao W. *et al.* 2005b, Guu *et al.* 2009, Yamashita *et al.* 2009, Xing *et al.* 2010, Xing *et al.* 2011, Jariyapong *et al.* 2013). The first selected position, Y485C, was previously used as the insertion site to expose a foreign peptide on the surface of the nanocapsid. Y485 has also been described as an essential epitope for neutralizing antibody binding. The second epitope T489C, nearby Y485, was

primarily chosen because of the combined data indicating its importance in neutralizing antibody recognition and cell receptor binding. The third site, S533 was selected because it was distal to nanocapsid dimer interface, facing the 5-fold symmetry axis. In addition, 533C is proximal to amino acids structurally associated with binding a neutralizing antibody, Hep224. The fourth site, 573C, also distant from the dimer interface is adjacent to a cell-receptor binding region. Like S533C, the fifth mutation site, T586C, was selected because it is adjacent to cell receptor and Hep224 binding regions. T586 is also close to the nanocapsid C-terminus, which was an effective insertion site for foreign epitope exposure in previous experiments.

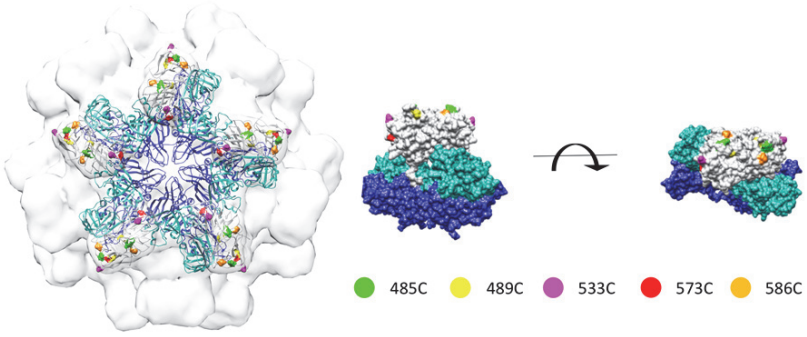

FIGURE 5 Nanocapsid cysteine replacement sites. Assembled nanocapsid (left) and dimer subunits (middle and right) are presented (subunits are not sized to scale). S-, M- and P-domain are dark blue, light blue, and gray, respectively. Surface rendition of assembled nanocapsid and nanocapsid subunits generated in Chimera using PDB 2ZTN.

Primers were designed for site-directed mutagenesis in to a baculovirus transfer vector containing the nanocapsid sequence insert, pFastBac1/dORF2-HEV. These plasmids were subsequently amplified in DH5α cells, purified, and sequenced. Sequencing results confirmed that each pFastBac1/dORF2-HEV plasmid contained the appropriate cysteine replacement sequence while the rest of the sequence remained unchanged. Subsequent steps towards cysteine-replaced nanocapsid (cys-nanocapsid) production were carried out using modified Bac-to-Bac Expression protocols (I). For nanocapsid expression, baculoviruses with cys-nanocapsid insert were used to inoculate *Tn5* cells. Collection and purification 6-7 days post *Tn5* cell infection resulted in the best yield, similar to that of WT nanocapsids.

All five of the purified cys-nanocapsids exhibited indistinguishable features to native nanocapsids in terms of solubility/dispersion in solution, SDS-PAGE banding at 52 kDa, and spiked-icosahedral capsid structure in EM. This suggested that none of the P-domain cysteine mutations affected capsid assembly, structure, or size. Hence, each of the assembled nanocapsids displays exactly 60 symmetric copies of cysteine in distinct positions for each mutant.

Unlike cysteine engineering studies with CPMV (Wang Q. *et al.* 2002, Wang F. *et al.* 2013), cysteine replacement on solvent-exposed nanocapsid residues did not require heavy reducing agents for production and no increased aggregation or precipitation was observed. This could result from structural differences between CPMV and HEV nanocapsid. The CPMV forms a relatively smooth icosahedral capsid with a large surface area such that chemical interactions on the capsid surface may affect the overall capsid structure. Conversely, the spiked protrusions on nanocapsids may make it less likely for solvent-exposed cysteines to participate in intermolecular disulfide linkage. Moreover, some disulfide linkage between cysteine residues on the HEV nanocapsid would not likely affect capsid assembly unless it were to occur at the dimer interface.

5.1.2 Cysteine exposure for conjugation

Each of the cys-nanocapsid constructs were conjugated to maleimide-functionalized biotin resulting in covalent biotinylation at the nanocapsid cysteine site. EM imaging post conjugation suggested all five of the nanocapsids were structurally unaffected by maleimide-biotin conjugation. SDS-PAGE followed by Western blot using a streptavidin-HRP was carried out to determine if each nanocapsid had sufficient cysteine exposure for maleimide conjugation and to compare relative conjugation levels between mutants (I, Fig. 2A). All five HEV-cys nanocapsids had a strong chemiluminescent signal at 52 kDa, while native HEV nanocapsid had no signal. Importantly, nanocapsid with a cysteine replacement at N573 (HEV-573C) exhibited the highest streptavidin binding signal compared with the other four mutants. Coomassie blue staining of the SDS-PAGE gel used in Western blotting suggested there was no difference between capsid protein concentration (I, Fig. 1a). Because SDS-PAGE reduces nanocapsids to a denatured monomeric state (maintaining covalent conjugation interactions), it was considered that there may be differences in biotin exposure between each of the denatured nanocapsid monomers, which would not reflect binding site exposure of the assembled capsid. To test this, nanocapsids were first disassembled in to dimers using previously described reducing and chelating conditions before maleimide-biotin conjugation. These nanocapsid dimers bound to maleimde-biotin were then assayed in Western blot, where streptavidin binding was nearly the same for all five mutants (I, Fig. 2A). It was therefore determined that the increased streptavidin binding signal observed for the HEV-573C was likely a result of increased binding site exposure in its assembled form.

Chemical modulation with maleimide-biotin did not affect capsid assembly. These results support earlier studies demonstrating the robust flexibility of the nanocapsid P-domain (Jariyapong *et al.* 2013). Western blotting indicated 573C had the highest binding site exposure (I). According to nanocapsid crystal structure, some of the nanocapsid cysteine replacement sites should be equally if not more solvent exposed than N573C. In considering an alternative explanation for the high streptavidin binding signal, we

hypothesized the location of neighboring 573C binding sites facing the 5-fold depression may be conducive to the formation of the native streptavidin-biotin tetrahedral complex. 5-fold interactions of 573C-bound AuNCs would be further evaluated in the next section (5.2).

5.1.3 Reduced HEV-specific antibody recognition

We inspected how cysteine replacement and cysteine conjugation might affect the affinity of HEV-specific antibodies, given N573 is located near residues previously associated with antibody recognition sites. *WT* nanocapsids, 573C nanocapsids, and maleimide-biotin conjugated nanocapsids were assayed with ELISA (I, Fig. 2B). Maleimide-biotin was used as a negative control. Two HEV-specific monoclonal antibody Fab fragments, HEP230 and HEP40-4, were tested for reactivity with the three different nanocapsids. In reactivity assays between nanocapsid and HEP40-4 Fab, maleimide-biotin bound and unbound 573C nancapsids were both similar in reactivity. Both bound and unbound 573C were slightly less reactive to HEP40-4 than native nanocapsid. Conversely, cysteine replacement and conjugation greatly affected HEP230 binding. Specifically, WT nanocapsids exhibited high reactivity to HEP230, 573C nanocapsids were only reactive at high nanocapsid concentration, and 573C nanocapsids bound to maleimide-biotin exhibited no reactivity with HEP230. These results suggested surface modulation could significantly alter the antibody recognition profile of nanocapsids.

The reactivity assay also indicated the Fab HEP230 binding site on nanocapsid was proximal to N573. 3D reconstruction was used to test the theory that HEP230 binds nanocapsids near N573 (I, Fig. 3). HEP230 Fab in complex with nanocapsids were imaged in cryo EM, after which images were processed for particle alignment and averaging, iterative refinement, and final 3D reconstruction. The resulting density map suggested a unique density, attributed to HEP230, positioned between two P-domain dimers at the periphery of the nanocapsid 5-fold depression. This data confirmed 573C conjugation occluded epitope-specific antibody recognition and resolved the binding site for HEP230.

These combined data supported antibody reactivity was dramatically affected by surface modulation. These findings suggest that interchangeable surface modulation techniques could be a solution for immune-evasion.

5.1.4 MDA-MB-231 breast cancer cell targeting

A previously described breast cancer targeting ligand, LXY30 (Xiao Wenwu *et al.* 2016), was conjugated to nanocapsid 573C in a two-step click-chemistry reaction . Developed using one-bead-one compound ligand discovery methods (Lam *et al.* 1997), LXY30 is a synthetic cyclized ligand that specifically targets α3β1, an integrin overexpressed in several types of tumor cells including breast cancer cells. Because LXY30 is cyclized via a disulfide bound, LXY30 could not

be directly functionalized with reactive maleimide. Instead, LXY30 was functionalized with an alkyne group for covalent click-chemistry reactivity with azide-maleimide (I, Fig. 4). In our first conjugation attempt, we bound maleimide-azide to the nanocapsid 573C through maleimide-thiol coupling. Subsequently, we carried out a copper catalyzed click chemistry reaction with the alkyne functionalized LXY30. However, the reactive oxygen species resulting from the copper catalysis reaction likely destabilized the nanocapsid structure (I, Fig. 4C). Alternatively, we carried out an initial click chemistry reaction between alkyne-LXY30 and maleimide-azide to form maleimide-azide-alkyne-LXY30 (mal-LXY30), followed by mal-LXY30 conjugation to nanocapsid cysteine. This second reaction did not affect nanocapsid structure (I, Fig. 4B). Using the nanocapsids from the second reaction, targeting capacity of these LXY30-bound nanocapsids was tested in cells. Copper-free click chemistry reactions were also attempted, but there were some issues with synthesis stability and subsequent conjugation (data not shown).

The lysine residues of LXY30-bound and unbound nanocapsids were fluorescently labeled with Cy5.5-NHS dye, detectable in the far-red visible spectrum. Breast cancer cell lines, MDA-MB-231 were used as a cellular model for breast cancer tumor. Flow cytometry results demonstrated increased cell-binding of LXY30-bound nanocapsids than unbound nanocapsids (I, Fig. 5a). To determine whether LXY30-bound nanocapsids remained on the surface or entered cells, fluorescently labeled LXY30-bound and unbound nanocapsids were incubated with MDA-MB-231 cell monolayers for 1hr at 37°C (I, Fig. 4b). While some fluorescence was observed in the cells bound to LXY30-free nanocapsids, LXY30-bound nanocapsid binding substantially increased fluorescence signal inside cells, suggesting LXY30 modulation increased nanocapsid internalization.

5.1.5 Tumor targeting in mice with breast cancer tumor xenograft

Fluorescently labeled LXY30-bound and unbound nanocapsid were subsequently studied for targeting breast cancer in mouse models. The bound and unbound nanocapsids were separately subcutaneously delivery in to mice with MDA-MB-231 tumor xenograft; after which, mice were fluorescently imaged at various time points (I, Fig. 6). For LXY30-bound nanocapsid delivery, significant fluorescent signal was observed at the tumor site 1 and 6 h post-injection. While substantially decreased, fluorescent signal at the tumor site was still apparent 24 h post injection. Unbound nanocapsid delivery did not elicit fluorescent signal at the tumor site. For both bound and unbound nanocapsids, fluorescent signal was observed in the liver and spleen. This is a relatively common observation in nanotheranostic delivery as a function of nanoparticle size (Albanese *et al.* 2012, Kang *et al.* 2015). Ex vivo imaging suggested unbound nanocapsids were retained 48hr in liver and spleen tissue while LXY30-bound nanocapsids did not (data not shown). This suggested surface modulation with tumor targeting molecules may have reduced clearance by the liver and spleen, enhancing tumor tissue retention.

Nanocapsids bound to LXY30 targeting molecules specifically targeted breast cancer tumor cells, were internalized in to breast cancer cells, and detected breast cancer tumor in xenografted mice. Unbound nanocapsids did not detect tumor cells. Nanocapsids simultaneously stabilized site-specific targeting ligands and detection agents as a multifunctional theranostic tool, demonstrating successful tumor tissue targeting and detection *in vivo.*

5.1.6 Next generation nanocapsid delivery

While tumor targeting was successful, LXY30-bound and unbound nanocapsid cell-uptake was observed in the liver, spleen, and kidneys (I, Fig. 6). Internalization in liver and spleen tissue is not an abnormal feature of nanotheranostic delivery (Albanese *et al.* 2012, Kang *et al.* 2015). The size of non-continuous endothelia fenestrations in the liver and non-specific uptake of spleen and liver macrophages result in the uptake of various nanoparticles (Li S.D. and Huang 2008). Particularly with HEV nanocapsids, we might expect an increased tendency towards liver uptake as the liver is the native host reservoir for hepatic viruses. Therefore, it is important to consider options to reduce this non-specific tissue binding. Surface modulation near the cell receptor binding epitope of nanocapsid could be a mitigating step to reduce liver uptake. This modulation could be carried out through inserting additional cysteines at the cell-receptor domain and subsequent chemical modulation with moderately sized ligands. Previous single-site P-domain mutations affected hepatic cell binding (Guu *et al.* 2009, Yu H. *et al.* 2011a), suggesting genetic modification such as insertion, truncation, or replacement could greatly reduce hepatic cell-binding. In earlier nanocapsid insertion experiments, a 10 kDa truncation in the P-domain, including residues involved in cell receptor binding, did not affect capsid assembly. Another strategy under investigation is the conjugation or genetic insertion of anti-fouling peptides to prevent non-specific tissue uptake (Yu Q. *et al.* 2011b, Yu S.L. *et al.* 2011c).

As detailed in the introduction, nanocapsids can encapsulate nucleic acid through Ca^{2+} mediated assembly. In our Patent Review (II) and patent (Cheng R.H. *et al.* 2016), we depicted the capacity for nanocapsids to encapsulate detection molecules such as iron oxide, gold nanoparticles, and quantum dots. For example, tumor targeting nanocapsids encapsulating supramagnetic iron oxide particles could be detectable with MRI. Magnetic nanoparticles show excellent promise in diagnostic applications but many clinical efforts have been stifled by problems with toxicity, systemic clearance, and poor bio-distribution (Cole *et al.* 2011, Markides *et al.* 2012, Birkhauser *et al.* 2013, Laurent *et al.* 2014). As observed with nucleic acid packaging, nanocapsids would likely stabilize and protect iron oxide nanoparticles *in vivo*. In principle, targeted nanocapsids would prevent problems such as nanoparticle aggregation, systemic clearance, and most importantly, reduce dosage by directing nanoparticles to the tumor site. Benefits of encapsulating iron oxide in tumor targeted nanocapsids carry over to therapeutic uses. Magnetic field induced hyperthermia is a well-studied phenomenon where external magnetic fields at a specific radiofrequency causes

iron oxide nanoparticles to heat up, damaging nearby tissue (Bañobre-López *et al.* 2013, Hervault and Thanh 2014). Directed lasers and tumor targeting help to localize heat induced cell death at the tumor site. Iron oxide nanoparticle encapsulation has been demonstrated with plant-based Brome Mosaic Virus nanoparticles (BMV LPs) through pH and ionic strength adjustment (Huang *et al.* 2007). Unlike HEV VLP production, live BMVs are produced followed by pH-based disassembly and RNA separation, such that assemblies have not been optimized for non-infectious protein-based production and empty particle formation. The HEV nanocapsid sequence is optimized to *not* encapsulate virus-RNA, forming highly stable non-infectious capsids capable of reversible *in vitro* assembly through cation mediation.

The immunogenicity of nanocapsids is also an important consideration for drug delivery as outlined in the introduction. The antibody reactivity tests suggest chemical modulation with small molecules greatly impacts antibody recognition. Because chemical conjugation is a relatively quick, one to two step process, surface modulation on alternating solvent exposed epitopes could aid in immune evasion. Previously, bioconjugation strategies have been shown to reduce immune recognition of viral vectors. In two separate examples, adeno-associated virus (AAV) vectors were chemically conjugated to glycan to form arginine adducts (Horowitz *et al.* 2011) as well as PEG via acylation of primary amine groups (i.e. lysine residues) on AAV (Lee *et al.* 2005). For both chemically modified AAV vectors, antibody neutralization was moderately to significantly reduced. In principle, antibody neutralization could be evaded by similar chemical modulation steps, with alternating binding sites in between administrations. This alternation would change the surface exposed and occluded epitopes available for immune detection in subsequent nanocapsid administrations.

In contrast to these obstacles, the inherent immunogenicity of virus-derived particles is being explored as a tool to elicit a tumor-specific adaptive immune response (Han *et al.* 2014, Lizotte *et al.* 2016). HEV nanocapsid immunogenicity stems from its repeated-symmetric protein subunits, of which host immune systems are adapted to recognize. While immunogenicity can be problematic for tumor delivery in some contexts, it is a tremendous advantage in cancer immunotherapy. The size-based passive transport of nanocapsid results in uptake in lymphatic tissue, where dendritic and CD8 immune cells are located (Bachmann and Jennings 2010). As previously illustrated (Takamura *et al.* 2004), nanocapsids recombined with surface exposed foreign peptides elicit a strong humoral and cytotoxic lymphatic response specifically to the foreign peptide insert. Previously, CpG (immune activating compounds) and tumor-antigens have been conjugated to protein-based nanoparticles to elicit a tumor-specific immune response (Molino *et al.* 2013). A similar strategy could be employed with nanocapsids with the advanced step of oral targeted delivery. Made possible by the flexible nanocapsid P-domain, nanocapsids could conjugate a ligand specific to mucosal lymphatic tissue such as Co1 (Kim S.H. *et al.* 2012) together with CpG and tumor antigen modulation. In principle,

such modulation would allow nanocapsids to localize to mucosal immune cells to elicit a tumor-specific immune response.

5.2 Conjugation methods and structure determination of nanocapsid bound to gold nanocluster

5.2.1 Au_{102} conjugation to nanocapsid

We pursued thiolate-protected gold nanocluster (AuNC) conjugation to solvent-exposed cysteine engineered on the nanocapsid P-domain (III, Fig. 1A-B). A 1.5 nm AuNC, Au_{102}(*p*MBA)$_{44}$ or Au_{102}, was chemically conjugated to nanocapsid cysteine in two forms: direct ligand exchange (Murray place exchange) and thiol-maleimide coupling (III, Fig. 1C). For direct ligand exchange, a thiolate ligand on Au_{102} was replaced with a nanocapsid cysteine, positioning gold atoms in direct contact with the nanocapsid binding site. For maleimide-thiol coupling, Au_{102} was functionalized with *N*-(6-hydroxyhexyl)maleimide (C_6MI), placing a short linker between AuNC and the cysteine binding site. Figure 6 illustrates the two different cysteine conjugation methods. Conjugation was confirmed through size exclusion chromatography, spectrophotometry, non-reducing SDS-PAGE, and cryoEM (III, Fig. 2).

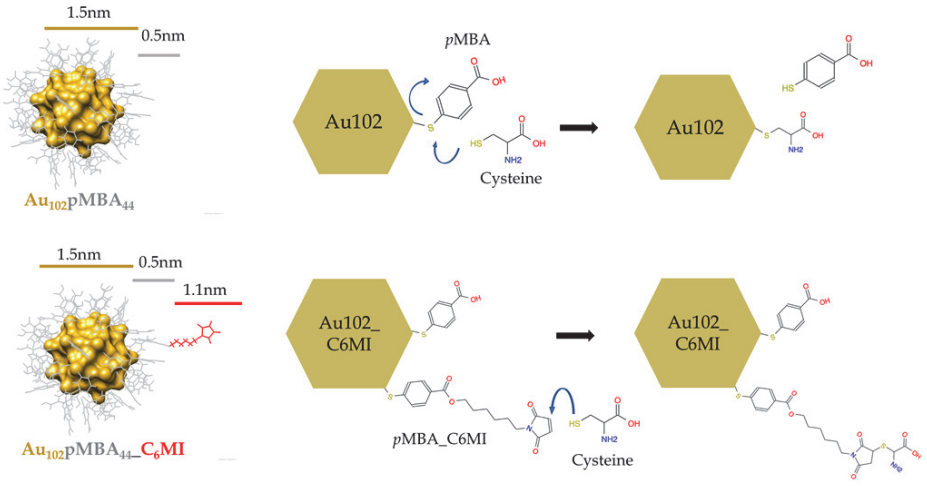

FIGURE 6 Gold nanoclusters Au_{102} (top) and Au_{102}C6MI (bottom). Left images depict Au_{102} crystal structure without (top) and with C6MI linker (bottom). Au_{102} crystal structure coordinates (Jadzinsky *et al.* 2007) Right images illustrate place exchange with Au_{102} (top) and maleimide-thiol coupling with Au_{102}C6MI (bottom).

Size exclusion with S-500 Sephacryl resin packed in chromatography columns was used to separate unbound AuNC. Spectrophotometry values at $A_{420\ nm}$ and $A_{280\ nm}$ were measured to calculate the molar concentrations of nanocapsid protein and AuNC (Ackerson *et al.* 2010a, Hulkko *et al.* 2011). The molar ratio of AuNC to binding site was used to determine average occupancy of AuNC on nanocapsid binding sites. The approximate percent occupancy of Au_{102} was 13.1% and 18.9% after 5 hour and overnight conjugation, respectively. $Au_{102}C_6MI$ occupancy was 35.5% and 22.1%, respectively (III, Fig. 2C). This suggested that $Au_{102}C_6MI$ conjugation was more efficient over short time periods but became less efficient over longer conjugation periods. Conversely, Au_{102} conjugation had increased binding efficiency over longer conjugation time. Following size exclusion, non-reducing SDS-PAGE results (III, Fig. 2D-2E) showed up-shifted brownish-colored band around 56 kDa, indicative of AuNC-nanocapsid complex. Both a 52 kDa band, reflecting the size of nanocapsid, as well as 56 kDa band were observed following Coomassie blue staining. The relative banding ratios observed in the non-reducing SDS-PAGE results supported our spectrophotometry results.

Precipitation studies suggested decreased $Au_{102}C_6MI$ conjugation efficiency may result from decreased solubility of $Au_{102}C_6MI$ over time (III, Fig. 2H), whereas non-functionalized Au_{102} remained relatively soluble over time. In particular, Tris-HCl pH 7.5 caused the most precipitation for $Au_{102}C_6MI$. CryoEM was used to inspect the nanocapsid structure and presence of AuNC on the nanocapsid surface (III, Fig. 2F). Interestingly, nanocapsids conjugated in MES pH 6.5 were more dispersed than nanocapsids conjugated in Tris-NaCl pH 7.5, which appeared to aggregate in cryoEM (III, Fig. 2G). This aggregation may result from the same properties that cause $Au_{102}C_6MI$ to precipitate in Tris-HCl. While the source of precipitation is not completely known, we hypothesized the hydrophobicity of C_6MI causes it to interact with other functionalized linkers and aggregate in solution over time. It is important to point out that the number of C_6MI linkers is not homogenous among clusters, and unpublished experiments have shown that an increase in C_6MI linkers results in increased precipitation. It is therefore likely, over the course of a conjugation reaction, that AuNCs with a higher number of C_6MI linkers precipitate more quickly than those with less linkers. Maleimide ring hydrolysis could also contribute to precipitation, which has shown to occur over extended periods in solution (Lyon *et al.* 2014). We also hypothesized that the increased precipitation observed in Tris-HCl buffer may be a consequence of HCl protonation of AuNCs based on previous data suggesting an increase in *p*MBA ligand protonation caused decreased AuNC solubility (Koivisto *et al.* 2016).

It should be taken into account that maleimide binding is not solely restricted to cysteine reactivity. As a nucleophilic reagent, maleimide can also conjugate primary amines such as lysines. Conventional wisdom suggests lysine reactivity is only favorable at or above pH 8. However, given enough time, lysine conjugation could occur sooner. Cowpea Mosaic Virus conjugation studies suggests maleimide can also bind surface lysines at pH 7, requiring initial lysine conjugation or amino acid replacement to prevent it (Strable and

Finn 2009). While this could occur with nanocapsid conjugation as well, given the presence of exposed lysine residues, it is likely at pH 6.5, exposed cysteine residues are significantly more favorable than lysine residues for maleimide conjugation.

5.2.2 Rigid modelling predicts ring formation at 5-fold symmetry axis

For Au_{102} conjugation via direct place exchange, nanocapsid cysteine binding sites were the assumed position of AuNC densities. However, the position of AuNC densities following $Au_{102}C_6MI$ (maleimide thiol coupling) conjugation was not as predictable given the linker distance between maleimide and cysteine. To inspect prospective positions of gold densities on the nanocapsid surface, rigid modelling was carried out based on spatial and atomic parameters of AuNC and nanocapsid (III, Fig. 3). Nanocapsid was represented as HEV-VLP crystal structure and AuNC core density was depicted as a spherical probe, sized according the atomic density of Au with Gaussian distribution. The probe size was represented as a specified diameter range to account for variations in the protective monolayer behavior. The probe position was limited to within a distance range from the cysteine binding site that reflected the size of the linker. This range was increased for the second and third model to account for potential nanocapsid structural changes that could slightly reposition the cysteine binding sites. Lastly, the position of gold density probes was restricted to only positions that had contact between probe surface and nanocapsid surface, and without atomic overlap. In all three models, the most probable gold density positions were localized to the nanocapsid 5-fold axis (III, Fig. 3). In the first two models, a ring-shaped density hovers above the nanocapsid 5-fold density with a hole in the middle, whereas the 3rd model shows all five densities in direct contact, merging as a single density above the 5-fold axis. The distance parameters for the first model fit best with known linker length, AuNC crystal structure, and binding site. In the second and third models, the third being the most extreme, were generated to reflect potential structural movement following conjugation that would cause a slight change in the cysteine binding site. This modeling consistently reflected gold densities hovering slight above the nanocapsid 5-fold symmetry axis, forming a circular ring-like structure.

5.2.3 3D reconstruction reveals a 5-fold ring density

CryoEM micrographs of $Au_{102}C_6MI$ were processed for refinement and single particle reconstruction (SPR). We acquired images close to focus and with more defocus for qualitative assessment of gold conjugation. Similar to previously described results (Sexton and Ackerson 2010), AuNCs were better resolved close to focus (0.5-1.5 µm defocus), whereas proteins display better contrast between 2–4 µm defocus (Fig. 7). In the early phase, we used EMAN 2.1 semi-automated boxing STORM software to select particles for reconstruction. AuNC densities did occasionally affect alignment, requiring the manual filtering

and/or re-centering of particles. AuNC densities also resulted in poor automated CTF correction with EMAN 2.1, so manual CTF correction with EMAN 1.9 was used. In the initial reconstruction phase, we used StartIcos (EMAN 1.9) from which a low-resolution volume map resembling that of native HEV-VLP T=1 crystal structure was generated. Later, we generated several initial models through the EMAN 2.1 e2initialmodel program to run refinement in parallel, confirming crude 3D reconstructed maps were stable. We carried out this course refinement to ~20 Å resolution, only keeping the top half of high scoring particles within one standard deviation of the population. Through the course of early refinement, it became apparent that heterogeneous AuNC binding required variability analysis. After confirmation that the map was stable over refinement and fourier shell curve showed consistent convergence, we reduced the angular step and low pass filter, reintroducing more particles in refinement. Early in refinement, a unique high intensity volume appeared in the 5-fold symmetry axis. To check whether this 5-fold density was an artifact of our reconstruction process, we processed cryoEM datasets for Au_{102}-bound and unbound-nanocapsids for 3D reconstruction and refinement. No high intensity 5- fold volumes were observed in the two other maps, suggesting the 5-fold density was unique to $Au_{102}C_6MI$-bound nanocapsids.

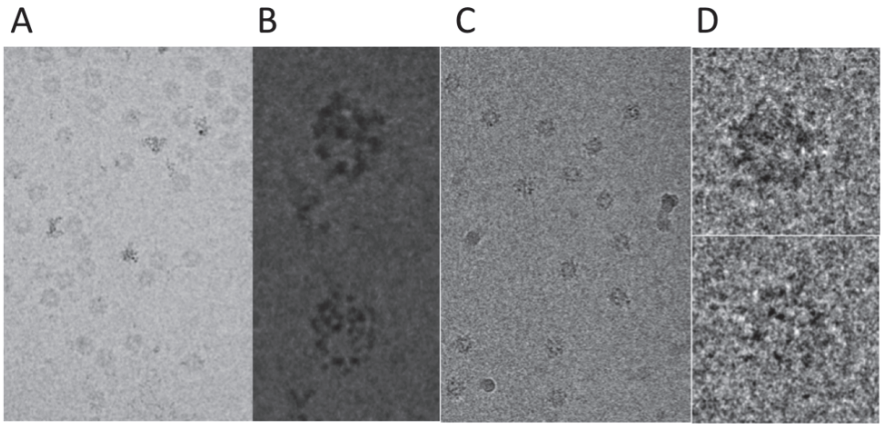

FIGURE 7 CryoEM images of nanocapsid conjugated to AuNC: (A-B) $Au_{102}C_6MI$ and (C-D) Au_{102}. (B and D) show defocus pairs of the same particle. Top images are taken with 3–4 μm defocus and bottom images are taken close to focus (0.5–1.5 μm).

To better resolve the unique 5-fold density, boxed particles were then processed using PFT (polar fourier transfer) methods to separate subpopulations by diameter via scaling measurements. Once establishing a better resolved 3D map, particles imaged with the same defocus were screened through 2D thresholding for discrete high intensity volumes (associated with AuNCs) and were isolated for further refinement. Particles were then assigned

individual orientation and center assignments for several iterations using PFT methods. Our final 3D structure, approximately 12.8 Å resolution, revealed five high density volumes at the 5-fold. These densities reflected the approximate size of AuNC densities, forming a ring-like shape around the 5-fold symmetry center. Difference imaging suggested these densities were in contact with nanocapsid residues that encircled the 5-fold center. Distance measurements from the 573C binding sites to the high intensity volumes were compatible with the known crystal structure and linker length $Au_{102}C_6MI$.

Rigid modeling data supported formation of a 5-fold ring of AuNC densities surrounding the 5-fold symmetry center. The known crystal structure of nanocapsids supports the finding that AuNCs tend to associate with the nanocapsid 5-fold. On the surface of the S-domain, hydrophobic residues surrounding the nanocapsid 5-fold axis are key to capsid assembly. The hydrophobic C6MI linker on AuNCs would likely participate in attractive hydrophobic interactions with hydrophobic residues in the nanocapsid 5-fold. The combination of hydrophobic interactions between neighboring AuNC clusters in addition to hydrophobic interactions with S-domain residues supports the ring cluster formation at the nanocapsid 5-fold revealed in 3D reconstruction. Depicting these interactions between AuNCs and the protein surface are crucial to ligand design and tuning the chemical surface of nanocapsids.

As previously metioned, we observed heterogenous AuNC binding to nanocapsids such that bound-AuNC was not evenly distributed among nanocapsids. Qualitative TEM results suggested about 25% of nanocapsids had a high number of AuNC attributable gold densities. The imposed icosahedral symmetry in standard refinement depicts 100% binding site occupancy. Given our spectrophotometry, SDS-PAGE and TEM data that suggest otherwise, we attempted reconstruction without imposed symmetry. We used the top 25% particles with a high number of AuNC densities to run a relaxed symmetry reconstruction and refinement (III, Fig. 5B). According to these results, approximately 40–70% of the binding sites were occupied. These results suggested, more than one AuNC particle bound each 5-fold axes on average. These results were distinct from the "all-or-nothing" occupancy observed in previous AuNC conjugation studies with enterovirus (Marjomaki *et al.* 2014).

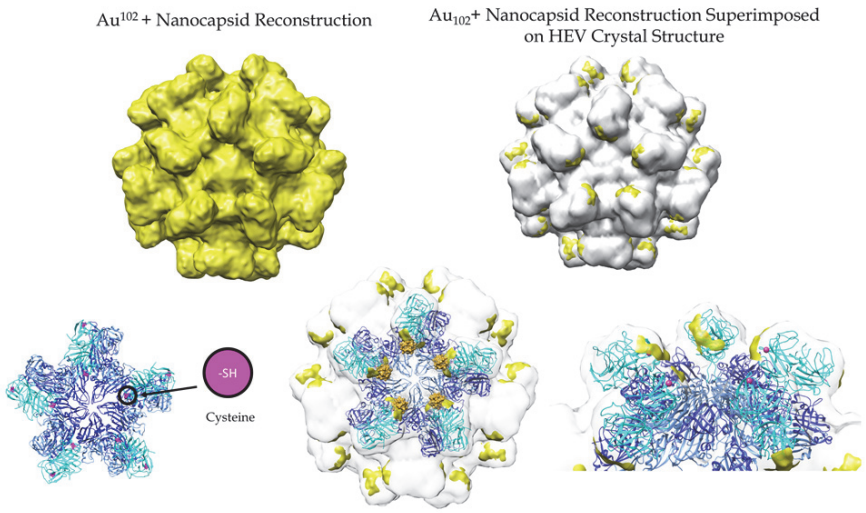

FIGURE 8 Reconstruction and modelling of Au_{102}-bound nanocapsid. 3D reconstruction of nanocapsid bound to Au_{102} (yellow). In the superimposed map (top, right) Au_{102}-bound nanocapsid (yellow) and surface rendered crystal structure (gray) appear to coincide with position of cysteine site (bottom left in pink). Lower image shows a nanocapsid pentamer docked to superimposed map, where the gold crystal structure is also overlapped with unique reconstructed densities. Images generated in UCSF chimera with PDB 2ZTN (Wang C.Y. *et al.* 2008) and Au_{102} crystal structure coordinates (Jadzinsky *et al.* 2007)

Similar methods of reconstruction are ongoing for Au_{102} conjugated nanocapsids. While still in early refinement stage, a preliminary 3D reconstruction at around 20 Å resolution did show unique protrusion in the 573C binding site region. No 5-fold densities were observed as seen with Au_{102}_C_6MI conjugation. Difference mapping between the unbound crystal structure and Au_{102} 3D reconstruction displays an extended density just under the dimer tips facing the 5-fold center (Fig. 8). While this protrusion could be attributed to AuNC densities based on its location, the refinement stage is too preliminary to confirm such claims.

This work reports the first successful Murray place exchange conjugation of monolayer protected gold nanoclusters to an icosahedral macromolecular complex. In previous conjugation studies, AuNCs were bound to antibody fragments which were subsequently bound to N9 neuraminidase protomer for single particle reconstruction, demonstrating rigidity of protein bound AuNCs (Sexton and Ackerson 2010). In their publication, it was suggested larger macromolecules could be used for conjugation with the implementation of shorter linkers between conjugate gold nanoclusters and larger protein complexes. Our reconstruction results provide the first structural determination of an icosahedral complex directly conjugated to AuNCs through a short linker.

When considering this work, it is important to remember monolayer-protected gold nanoclusters (AuNCs) are distinct from commercially available

colloidal gold nanoparticles and commercial Nangold®. Being truly monodispersed (one size and one chemical composition) AuNCs form a single crystal structure in the solid phase which also informs the basis to understand their structure and function in the solution phase. This is in stark contrast to the better-known colloidal AuNPs that show 5-15% heterogeneity in size. With a defined AuNC structure, the specific position of bound AuNCs on the nanocapsid surface can be realized with high resolution cryoEM imaging and SPR.

A point that was not discussed in the submitted manuscript (III) was Ca^{2+} and Mg^{2+} induced precipitation of both functionalized and non-functionalized AuNCs. One of our interests in the AuNC conjugation is to study nanocaspid assembly and nucleic acid packaging in cryoEM using AuNC-bound nanocapsids. As previously described, reversible assembly of nanocapsid is a Ca^{2+} mediated process. We have observed concentration and buffer dependent precipitation of AuNCs (Fig. 9). This suggests the Ca^{2+} concentration for nanocapsid assembly must be sufficiently low to maintain AuNC solubility. Some groups have previously studied Ca^{2+} precipitation properties of colloidal AuNPs and even proposed such precipitation behavior as a diagnostic tool (Kim S. *et al.* 2009). It is well known that assembled hepatic virus capsids contain Ca^{2+} salt bridges, critical to capsid structure (Choi *et al.* 2005). These unique properties suggest interactions between Ca^{2+} mediated capsid formation and AuNC precipitation could provide interesting avenues of exploration.

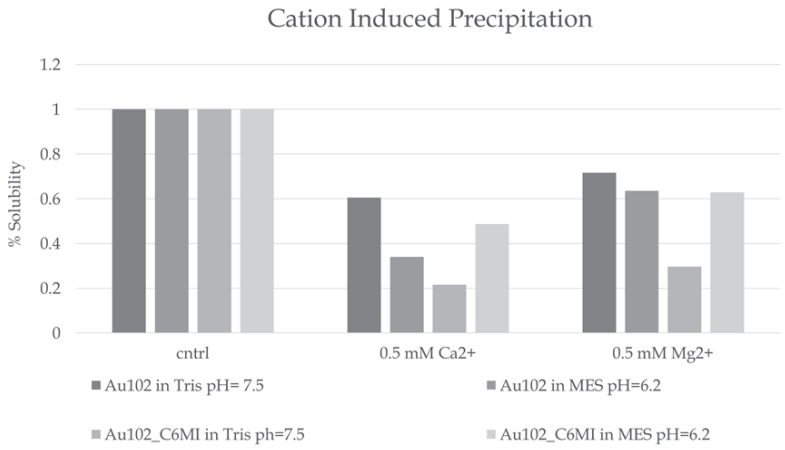

FIGURE 9 Ca^{2+} and Mg^{2+} precipitation. Prepared cations at concentrations near the threshold of complete precipitation comparing AuNCs and buffer conditions.

5.2.4 Imaging and theranostics with AuNC bound nanocapsids

An immediate application of AuNC-bound nanocapsids would be to use cryoEM tomography or Focused Ion Beam/Scanning Electron Microscopy (FIB/SEM) to observe nanocapsid internalization in cells, tumor spheroids, and other tissue samples. In most EM labeling techniques, gold-bound antibody or antibody fragments are used either *in situ* or post imbedding. As described in the introduction, these methods pose obstacles with permeability, degradation, epitope accessibility, and decreased resolution. These obstacles can be met with direct AuNC conjugation to the nanocapsid surface. Given the predictable orientations of monodispersed AuNCs on the nanocapsid surface, we could not only track cell entry, but also potentially observe disassembly or degradation events in different tissues. By testing various targeting ligands, we could begin to observe the specific entry and host-cell trafficking pathways elicited by target nanocapsid delivery.

Optical properties such as UV-Vis absorbance, surface plasmon resonance, and photothermal effects of some AuNPs have additional *in vivo* theranostic applications (Hu *et al.* 2006, Almeida *et al.* 2014, Key and Leary 2014, Zhang X.-D. *et al.* 2015). Most of these properties have been studied using colloidal gold AuNPs, lacking the molecule-like characteristics of AuNCs. A recent study described a small plasmonic AuNC, $Au_{\sim 250}pMBA_m$, where disulfide linkage between individual plasmonic $Au_{\sim 250}$ resulted in plasmonic coupling (Lahtinen *et al.* 2016). Plasmonic coupling resulted in a unique red-shifted UV-vis absorbance signal in the far-red and infrared spectrum. These absorbance spectra are particularly useful in biological imaging because of the low background light scattering, such that a specific absorbance signal in deep tissue samples can be observed. Ligand-exchange or maleimide thiol conjugation could be used to bind plasmonic AuNCs to the nanocapsid surface. In principle, attached AuNCs could be linked through disulfide bonding, such that the assembled AuNC-nanocapsid complex would exhibit unique optical properties characteristic of plasmonic coupling. $Au_{\sim 250}$ conjugation to nanocapsid cysteines has been successful as shown in SDS-PAGE results (Fig. 10A) and cryoEM (Fig. 10B). By determining the orientations of discrete AuNCs bound to large symmetric complexes, we have the potential to tune transitional light properties of AuNCs such as surface plasmon resonance, near-infrared absorption, fluorescence, and photothermal effects.

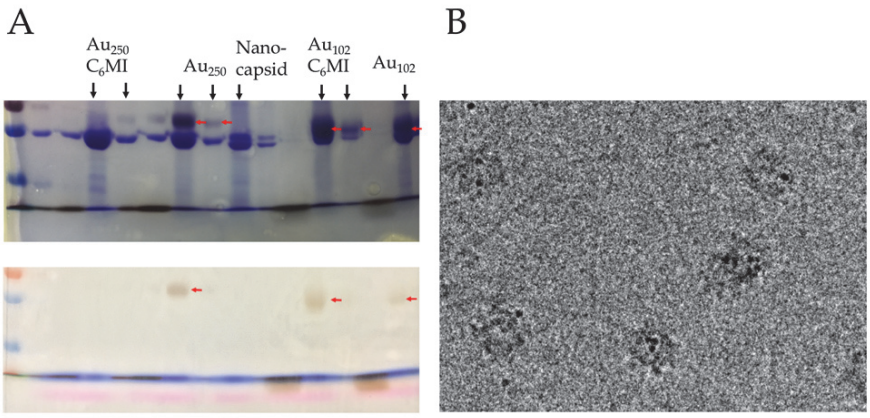

FIGURE 10 Nanocapsid conjugated to AuNC (A) SDS-PAGE stained (top) and unstained (bottom) of AuNC-bound nanocapsids. (B) CryoEM micrograph of $Au_{\sim 250}$ conjugation to nanocapsids. Au250 conjugation results in an upward band shift (red arrows) with slightly purple tint compared with Au_{102}.

5.3 Recombinant EV delivery

As previously mentioned, Hepatitis E Virus lacks an efficient cell model for infection studies. This deficiency limits studies in to mechanisms of native virus including cell-trafficking, genome packaging, release, and expression. Conversely, many enterovirus B subspecies (EVBs) have well described replicon-based cell models. In this study, a plasmid cassette (pCAS) containing Coxsackievirus B5 (CVB5) non-structural proteins (NSPs) was recombined structural proteins (SPs) from Echovirus 1 (EV1) to generate a recombinant EV1/CVB5 virus (EVCV). Unlike the EVBs used in the previous recombinant study mentioned in the introduction (2.4), EV1 does not share a host-cell receptor with CVB5. We were interested in distinguishing the role of SPs and NSPs in both infection kinetics and lytic vs non-lytic infection. Comparing the EVCV with parent viruses highlights which stages of infection are likely dependent on capsid structure and host-cell receptor binding vs. NSPs. We also compared infection with CVB3 to further study the impact of host-cell receptor on lytic vs. non-lytic infection phenotype. Like CVB5, CVB3 also binds CAR for host cell receptor-mediated entry, but does not bind host-cell receptor DAF.

5.3.1 Parental and chimeric replicon-based virus production

In chemically competent *E. coli* cells, we amplified pSPORT replicon plasmids containing full length EV1 *Farouk* strain (pEV1) and CVB5 D*alldorf* strain (pCVB5), as well as the pEVCV clone containing native EV1 SPs and native CVB5 NSPs (Fig. 11). After screening, plasmids were separately transfected in

to *Green Monkey Kidney* (GMK) cells for respective virus production. Transfection with pEV1 induced complete GMK lysis less than 48 h post transfection. pCVB5 transfection require two supernatant passaging steps on to fresh GMK cells to induce cell lysis, and exhibited increased cell-lysis efficiency after three passages. pEVCV required 2–3 passages to completely lyse cells. However, once a sufficient lytic effect was observed for EV1, CVB5 and EVCV, cell supernatant was used to scale up production. EV1 supernatant consistently elicited complete GMK cell lysis 24 h post inoculation; whereas EVCV and CVB5 took approximately 48–72 h for complete cell lysis. Following virus production, each of the constructs was purified through a series of ultracentrifugation gradient steps.

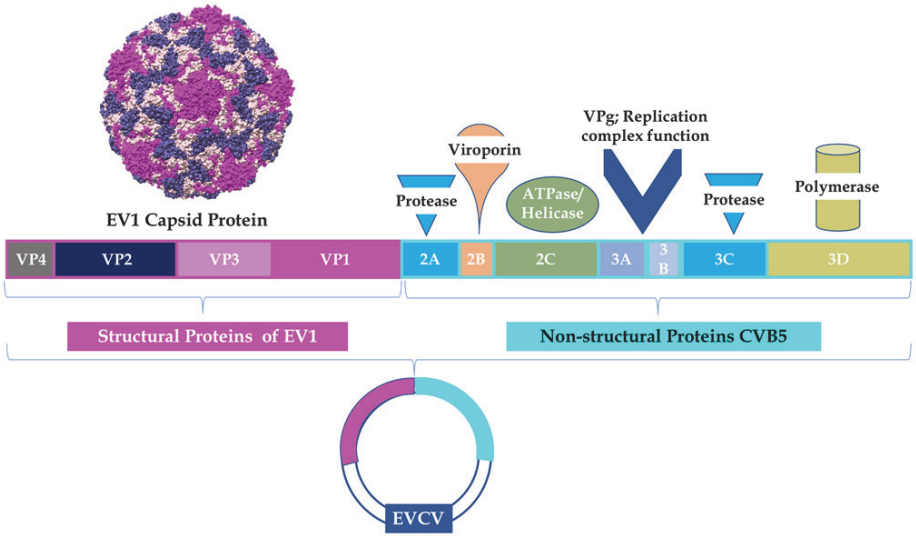

FIGURE 11 Schematic of recombinant virus EVCV. Structural proteins of EV1 recombined with non-structural proteins of CVB5.

5.3.2 Characterization of chimeric and parental virus

Spectrophotometry measurements at $A_{260\ nm}$ were used to assess the approximate number of RNA-containing capsids and infectivity tests were carried out in GMK cells (IV, Fig. 1A). SDS-PAGE confirmed the presence and relative purity of viral proteins (VPs) 1–3 (IV, Fig. 1B). EM imaging displayed intact viruses containing RNA from each of the respective clones (Fig. 11). According to these EM results, there was a limited number of empty EV1 capsids, whereas CVB5 production yielded a high percentage of empty capsids. To a lesser extent, this was also true for EVCV. The formation of empty capsids may have been an error of production or purification, though confocal microscopy results described later in this chapter seemed to support this trend, particularly for CVB5. Using 440 µg/mL EV1 and 870 µg/mL EVCV, infectivity results suggested EV1 and EVCV had comparable infectivity at 6.7 x 10^{10} and

1.3 x 10^{11} pfu/mL, respectively. Conversely, CVB5 concentration was about 1.35 mg/mL and yet its infectivity was almost two logs lower than EV1 and EVCV at 3.5 x 10^{9} pful/mL (IV, Fig. 1A).

In A549 cells, all three viruses exhibited cytolytic infection but infection kinetics were unique for CVB5 infection. Expressing both DAF and CAR receptors on their cell surface as "permissive cells", A549 cells were first tested for cell viability 12 and 24 h p.i. (IV, Fig. 2A). Using equal virus concentrations, infection kinetics of EVCV exhibited more similarities with EV1 infection than CVB5 infection. Both EV1 and EVCV infection lead to rapid cell death, such that approximately half of the cells were lysed within 12 hrs p.i. and completely lysed 24 hrs p.i. Conversely, 12 hrs p.i. with CVB5, approximately 70% of cells were viable. Complete cell death was not observed until approximately 72 hrs p.i.

Differences in infection kinetics, with respect to the viral replication timeline, were inspected in infected A549 cells immunolabeled with double stranded RNA (dsRNA) 6 h and 24 h p.i. (IV, Fig. 2B-C). After 6 h p.i., all cells infected with EV1 and EVCV showed signs of viral replication; whereas no dsRNA signal was observed with CVB5 infection. After one day, 20% of CVB5 infected cells had dsRNA signal (IV, Fig. 2B). Average intensity calculations of fluorescent dsRNA signal following infection with all three viruses suggested CVB5 and EVCV displayed a stronger dsRNA signal than EV1 (IV, Fig. 2C). Unlike EV1 and EVCV infected cells, much of the dsRNA signal was observed closer to the surface of CVB5 infected cells and suggested RNA replication was in the perinuclear region. A strong similarity between EV1 and EVCV infection compared with CVB5 infection might suggest that the host-cell receptor primarily determines the timeline for RNA replication and cytolysis. It appears that the level of viral genome replication might be higher in CVB5 and EVCV, indicating NSPs may influence the amount of RNA replication at later time points in virus lifecycle.

Subsequent infection studies in rhabdomyosarcoma (RD) cells demonstrated more similarities between EV1 and EVCV infection than CVB5 infection. Using ATP measurements, cell viability was measured 12 h and 24 h p.i. (IV, Fig. 3). EV1 and EVCV infection exhibited a cytolytic infection phenotype highly similar to that observed with A549 cells, though RD cells took a bit longer to completely lyse. Conversely, approximately 75% of RD cells 12 h and 70% of RD cells 24 h post CVB5 infection remained viable. 48 h post CVB5 infection, RD cell viability remained unchanged. This suggested CVB5 infection in RD cells resulted in a persistent phenotype, which was shown previously (Gullberg *et al.* 2010a).

5.3.3 Host-cell receptor mediated persistent infection

Low transient expression of CAR in RD cells is thought to be the source of persistent CVB5 infection (Argo *et al.* 1992, Gullberg *et al.* 2010a). CVB2 studies suggested the virus structural proteins, namely VP1, most strongly impacted infection phenotype (Gullberg *et al.* 2010b). After determining that EV1

infection elicited cell lysis in RD cells, we had a robust comparative model to distinguish the role of SPs and NSPs in infection phenotype. EVCV infection also elicited a cytolytic phenotype, suggesting the host-cell receptor mediated-entry was a probable trigger for infection phenotype as opposed to NSP interactions at later stages of infection. This finding was not necessarily expected given the presumed role NSPs play in shutting down host cell machinery and propagation of progeny viruses. These studies support previous findings of SP involvement in infection phenotype.

To test our hypothesis of host cell receptor-dependent infection phenotype, CVB5 and CVB3 infection were compared. While CVB5 can bind both DAF and CAR host-cell receptors, CVB3 only binds CAR. Post purification, both CVB3 and CVB5 were approximately 1 mg/mL, but again, CVB5 was approximately two logs lower in infectivity of GMK cells at 1.3×10^{10} vs. CVB3 which was 1.1×10^{12} (IV, Fig. 4A). Both CVBs induced A549 cell lysis 96h p.i (IV, Fig. 4B). However, 24h p.i., CVB3 had caused almost 100% cell death while approximately 62% of CVB5 cells were still viable. As expected, both CVB3 and CVB5 exhibited a persistent infection phenotype in RD cells with no apparent cytolysis in as long as 9 days p.i (IV, Fig. 5).

Because CVB5 infection kinetics were delayed compared to those of CVB3 infection, dsRNA immunolabeling used to compare CVB5, EV1 and EVCV virus replication was implemented to compare CVB5 with CVB3 replicaiton (IV, Fig. 6). CVB capsid proteins were also immunolabeled for these assays. After 6 h p.i., 34% of CVB3 infected A549 cells had detectible dsRNA, as opposed to 11% in CVB5 infected cells. Unlike the EV1/EVCV studies, CVB5 replication appeared to catch up with CVB3 after 12 h p.i. in A549 cells where approximately 45% cells had dsRNA signal. Despite the equivalent percentage of cells exhibiting dsRNA replication, 24h p.i., CVB3 lysed nearly 100% of A549 cells as opposed to CVB5 lysing less than 40% of cells. In the first 48 h p.i., 10% of CVB5 and CVB3 infected RD cells were replication and CVB capsid positive. At 96 h p.i., about 58% CVB5 infected RD cells were capsid positive, whereas only 25% of CVB3 infected RD cells were capsid positive 96h p.i.

Infection with all four virus constructs caused lytic infection in permissive A549 cells that express cell-surface CAR. Compared with EV1, EVCV, and CVB3, CVB5 exhibited lower infectivity, and slower rate of lysis and replication in A549 cells. Lytic RD cell infection was observed for EV1 and EVCV, but not for CVB3 or CVB5. EVCV data indicates SPs, specifically cell receptor binding, as the most likely driving force of infection kinetics and persistent infection than NSPs. In addition to cell receptor binding, it cannot be ruled out that downstream SP interactions influenced some aspects of infection phenotype. For example, Enterovirus SPs VP1-3 have been shown to induce apoptotic responses (Henke *et al.* 2000, Peng *et al.* 2004, Gullberg *et al.* 2010b). As previously mentioned, only a small subpopulation of RD cells express CAR on their cell surface. While CVB5 can also bind DAF host-cell receptors, CVB3 only binds CAR. Initially, CVB5 and CVB3 have persistent infection in about 10% of cells, which is likely representative of the small subpopulation of cells expressing CAR on their cell surface. Previous studies have suggested DAF

may sequester virus on the cell surface, without permitting cell-entry or the structural changes necessary for infection (Milstone *et al.* 2005). During virus propagation, it is possible that CVB5 capsids are sequestered on the surface of other RD cells lacking CAR, while CVB3 capsids are only observed within the population of cells expressing CAR. This would account for the percentage of capsid positive CVB5 infected RD cells being much higher than the percentage of replication positive cells. This may also explain the delayed infection kinetics of CVB5, where some CVB5 may be halted in virus replication and propagation due to sequestration by DAF receptor binding.

Empty capsid production may also be partly attributed to CVB5 NSPs as EVCV seemed to also produce a higher number of empty capsids than observed with EV1 (Fig. 12). Though less significant than the host-cell receptor differences, NSPs appeared to affect the level of RNA replication, suggesting CVB5 NSPs could induce more RNA replication than EV1 NSPs. In the preceding work from which the CVB5 NSP pCAS cassette was first introduced, serial passaging steps were required to produce a cytopathic effect (CPE) (Jonsson N. *et al.* 2015b). This finding was similar to observations of CVB5 and EVCV, while EV1 did not require serial passaging and caused complete cell lysis within the first passage. While these findings require further investigation, NSPs may be responsible for this difference in cytolysis kinetics.

A more thorough investigation with deep sequencing might help to identify key proteins responsible for adaptations in receptor binding. Recently, the Lindberg lab carried out complete transcriptome sequencing of EVB infected RD cells to identify how lytic and non-lytic infection phenotypes impact transcription in the host cell (Savneby *et al.* 2016). No definitive findings were proposed in this study; though several host-transcripts were identified as indicators for lytic vs. non-lytic infected cells. Researchers also hypothesized that protease NSPs 2A and/or 3C could promote cell lysis by downregulated host RNA expression. Deep sequencing studies might also provide evidence for adaptation during cell passaging following initial transfection. Differentiating adaptive mutations between various EVB transfected cell lines would provide a more robust mechanism for host-cell dependent adaptations.

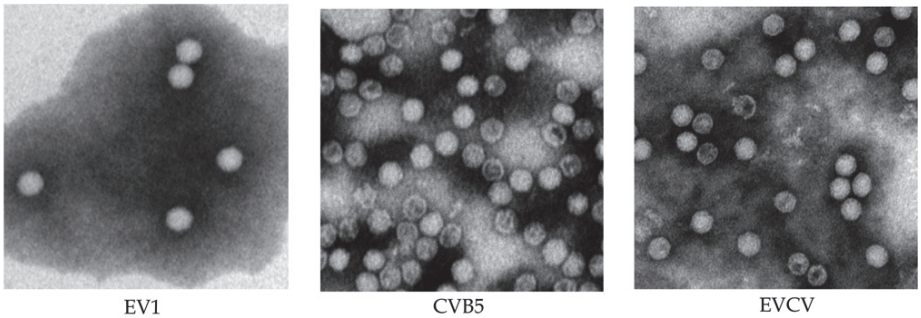

FIGURE 12 TEM images of EVB constructs generated from pSPORT plasmid. CVB5 and EVCV populations appear to have representative empty capsids.

5.3.4 Connecting host-cell mediated entry and infection efficiency with theranostics

While most biotechnology advancements attributable to fundamental cellular and molecular biology research are often unpredictable at the time of discovery, we can already start to draw connections between this work and theranostic development. In tumor-targeted ligand design, much focus is placed on increasing affinity to a specific cell-receptor. The results from this this study suggest, in a single population of cells, affinity for multiple receptors can affect cell-internalization efficiency and gene expression. Hence, interactions such as competing binding site, internalization, and host-cell trafficking should be optimized and evaluated for tumor targeted nanocapsids. Conversely, if cell internalization is not preferred, cell-receptor targets should be limited to those that do not permit internalization, as observed with DAF binding.

With follow-up deep sequencing studies, cell-dependent adaptation could point to specific protein changes that promote persistent vs lytic infection. The difference between CVB5 and CVB3 was clear in this case suggesting that the differential usage of receptors leads to differences in RNA and capsid production, and perhaps in RNA packaging efficiency. To address previous research indicating 5′ deletion of the viral genome led to infection persistence, deep sequencing could be carried out over several days of virus infection in RD cell culture. Understanding the tissue tropism and tissue-specific host cell receptor-mediated trafficking provides insight to optimize selection of tumor-specific cell receptor targets.

6 CONCLUSIONS

With the ambition to investigate and finely tune theranostic delivery platform, this thesis synthesizes virus and virus-like particle based methods in cell delivery providing a basis of information and proof-of-concept studies to propel theranostic applications of a nanocapsid platform.
The conclusions reached in this thesis were:

I Five HEV nanocapsid subunits engineered with a single solvent-exposed cysteine assembled in to T=1 icosahedral nanocapsids with 60 symmetric cysteine residues. Post cysteine modification and conjugation nanocapsids maintained icosahedral structure. Of the maleimide-biotin bound nanocapsids, 573C exhibited ideal binding site exposure. Unbound and maleimide-biotin bound 573C nanocapsids had little to no reactivity with anti-HEV antibody Fab, HEP230, suggesting native N573C and/or nearby residues were involved with HEP230 affinity. 3D reconstruction results supported this hypothesis.

II Nanocapsids specifically targeted tumor cells *in vivo* and in animal models. Nanocapsid 573C was successfully modulated with a breast cancer targeting ligand, LXY30, through two step conjugation. Fluorescent LXY30-bound nanocapsid exhibited a significantly higher level of breast cancer cell binding and internalization than unbound nanocapsid. Breast cancer tumor xenografted mice administered with LXY30-bound nanocapsids displayed tumor-xenograft specific binding and cell uptake 1 h, 6 h, 24 h post injection whereas unbound nanocapsids did not bind tumor xenografts. Non-specific liver and spleen uptake of LXY30-bound and unbound nanocapsids was observed.

III Au_{102} conjugation to nanocapsid was the first example of direct place exchange conjugation of thiolate-protected gold nanoclusters to a large icosahedral complex. Linker functionalized Au_{102}_C_6MI conjugation was more efficient than Au_{102} conjugation over short time, but tended to have

reduced conjugation efficiency over time due to precipitation. Au_{102} conjugation efficiency increased over itme. 3D reconstruction of Au_{102}_C_6MI conjugation to nanocapsid cysteine revealed 5 unique densities, attributed to Au_{102}, forming a ring above the 5-fold symmetry center. Independent rigid modeling supported these findings.

IV Chimeric virus EVCV properly assembled, encapsulating RNA. Recombinant EVCV more closely resembled EV1 than CVB5 in infection kinetics and phenotype suggesting NSPs did not strongly influence infection persistence in RD cells. CVB5 and CVB3 studies supported our hypothesis that differences in host-cell receptor binding may determine lystic vs persistent infection phenotype as well as infection kinetics. Sequencing studies would help confirm differential receptor usage and adaptation to viral persistency via 5′ deletion of the viral genome.

Acknowledgements

The research presented in this thesis was initiated by group leaders from University of Jyväskylä, Finland and University of California at Davis, USA between 2014-2017. Made possible through this international collaboration, this research was carried out with Department of Biological and Environmental Sciences, Department of Chemistry, and Department of Physics at the University of Jyväskylä, and the Department of Molecular and Cellular Biology at University of California at Davis. The supervisors who led this collaboration were Varpu, Marjomäki, Hannu Häkkinen, and R. Holland Cheng. These projects were funded by FiDiPro TEKES and the Academy of Finland.

First, I would like to thank my supervisor Adjunct Professor Varpu Marjomäki, without whom this collaboration could have never been realized. Thank you for taking me under your wing from the moment I joined your group, providing me with countless hours of mentorship and support. Your obligations in teaching, projects, and international collaboration have never prevented you from taking the time to provide me with guidance and enthusiasm. You have taught me many invaluable skills in science, collaboration, and what it means to be an exceptional mentor. Your passion for science and endless support for us, your students, has promoted a productive environment of friendship, teamwork, and enthusiasm for our projects. Words cannot express the gratitude I have for you welcoming me to your group and investing so much time and consideration in me as your student.

I want to express immense gratitude to my supervisor Professor Hannu Häkkinen, who has also mentored me throughout my PhD. Thank you for introducing me to a whole new field, and your willingness to guide me through unknown territory. Your passion and knowledge in your field, as well as your interest in stepping outside to seek interdisciplinary collaboration, is truly inspiring. Thank you for your patience in navigating me through the necessary fundamentals, providing insight in to your field. I cannot thank you enough for supporting my relocation to Davis to continue research there as well as providing me with your and your colleague's expertise along the way.

I want to thank my supervisor R. Holland Cheng, who first introduced me to this opportunity in University of Jyväskylä Finland. Professor Cheng, thank you for inviting me to your lab as an undergraduate and providing me a path to pursue these projects in a PhD program. Your enthusiasm for new opportunity and interdisciplinary collaborations has kept the projects exciting and innovative. Thank you for having so much confidence in me to embark on new projects and ideas. I also want to thank you for supervising this successful collaboration between the University of Jyväskylä and UC Davis.

I am very grateful to the thesis reviewers Professor Mauri Kostiainen and Assistant Professor Christopher Ackerson. I was very fortunate to receive your extensive review under the short time constraints. Despite the exceptionally short timeline, your comments and revisions were incredibly thoughtful and comprehensive, helping to improve the quality, accuracy, and depth of my

thesis. I would also like to thank my thesis follow-up committee members Professor Vesa Hytönen and Professor Heikki Hyöty for offering sound recommendations to help guide the thesis. Thank you Vesa for making an extra effort to focus the research and offer your insight. I would also like to express my appreciation to Dr. John E. Johnson for accepting the invitation to serve as my opponent in the public examination of my thesis.

I have much love and appreciation for my colleagues and friends from the Marjomäki lab: Mira, Mari, Paula, Anni, Lassi, Moona, Visa and Maria who have been exceptionally welcoming and helpful throughout my time working in the Marjomaki lab. I have gotten to know these colleagues well and am privileged to call many of them friends. I have shared some of my most memorable experiences with many of you- thank you for making my experience one of a kind! I would like thank Tanja and Kirsi from Hannu's lab for regularly providing materials and spending time to help me understand and optimize the chemistry behind our bioconjugation work. I want to acknowledge Sami for putting extra time in to our most recent publication. I would also like to thank Janne Ihalainen for aiding my thesis work and graduation unit completion.

Mo Baikoghli, I could not have done this without you. Thank you for your endless support, thoughtfulness, and friendship throughout my time with you in UC Davis. You have been an amazing colleague both professionally and personally. I am so grateful to call you both a friend and co-worker, and I know we will continue to stay in touch long past our time together in Davis. I want to also acknowledge Prasida Holla who offered much of her time and advice in the lab, in writing, and in person. You are a very genuine, caring person and I am grateful for your friendship and mentorship.

I am indescribably thankful to my parents Mark and Kathleen for supporting me through each step of this program in countless ways. You're love and support gave me the confidence to pursue a PhD, inspiring me to seek new experiences and opportunities. Thank you for your exceptional professional and interpersonal guidance, listening to my complaints and excitement, as well as the scientific chats. You guys are truly the best parents out there. I also want to thank my amazing Mom, Christine, for your unconditional love and care through this process. Thank you for encouraging me to strive for a higher education, even when you would have preferred me to be close to home. Thank you for always believing in me, and boosting me up.

Lastly, words do not express how grateful I am for my loving boyfriend Michael, who has never stopped supporting me from abroad and close to home. I am lucky to be in love with my best and most supportive friend. Your understanding and selfless encouragement, even when it meant I would make our lives together significantly more complicated, mean the world to me. Thank you for staying by my side and making life more enjoyable than I've ever known.

YHTEENVETO (RÉSUMÉ IN FINNISH)

Nanokapsidien kehittely kohdennettavia lääkehoitoja varten

Syöpä ja geneettiset sairaudet ovat haastavia diagnosoida ja hoitaa koska näiden taustalla olevia molekyylejä tai niiden muutoksia voi olla vaikeita tunnistaa. Näiden sairauksien heterogeenisyyden vuoksi yleisessä käytössä olevat diagnosointimenetelmät ja hoitomuodot ovat tehottomia ja epäluotettavia. Tämän vuoksi niiden hoitoon on pyritty kehittämään molekyylitason menetelmiä. Lisäksi lääkemolekyylien parempi kohdennettavuus parantaisi saavutettavuutta ja hoitovastetta. Tehokkaampi targetointi myös lisäisi signaali-taustasuhdetta sekä hoitomolekyylien spesifisyyttä, vähentäisi lääkkeen pitoisuutta ja minimoisi sivuvaikutuksia. Yksilölliseen terapiaan kehiteltävät nanopartikkelit ovat nanokokoisia alustoja jotka stabiloivat lääkemolekyylejä kudostargetoinnissa. Virukset ovat luonnossa esiintyviä nanopartikkeleita ja valmiita kohdennettavia työkaluja yksilölliseen terapiaan. Vaikka virusten monistuminen ja siihen liittyvät patologiset prosessit eivät ole toivottavia lääkehoidoissa, virusten stabiilisuus, kudoskohdennuspotentiaali ja näiden pakkausominaisuudet ovat positiivisia seikkoja yksilöllisessä lääkehoidossa. Virustargetointitutkimukset voivat myös tuoda tärkeää uutta tietoa ja ideoita lääkehoitoihin. Tässä väitöskirjassa tutkitaan rekombinanttivirusten ja viruksista kehiteltyjen supramolekyylikompleksien käyttöä yksilöityihin lääkehoitoihin.

Väitöskirjan ensimmäinen osatyössä on kehitelty Hepatiitti E-viruksista (HEV) tuotettujen nanokapsidien käyttöä rintasyövän detektointiin ja hoitoon. HEV on ruoansulatuskanavan kautta infektoiva virus. HEV-viruksen kapsidiproteiinit muodostavat ei-infektiivisiä spontaanisti kasautuvia ikosahedraalisia kapsideja, jotka voivat kestää suoliston suurta hajottavaa proteaasimäärää ja matalaa pH:ta. Nanokapsidi kestää isojakin muokkauksia sen pintarakenteissa ilman suurempia muutoksia viruksen pakkautumisprosessissa. Tässä väitöskirjassa HEV-nanokapsidia muokattiin paremmin syöpäsoluihin kohdentuvaksi: nanokapsidiin lisättiin kysteiini. Työssä tuotettiin viisi erilaista potentiaalista kohtaa kysteiinille. Yksi näistä, 573C-mutantti osoittautui parhaimmaksi kysteiinisignaaliltaan. Tämä kysteiinikohta myös peitti immunologisen epitoopin, mikä olisi etu HEV-perusteisissa hoidoissa vähentäen suoraan HEV-kapsidiin kohdistuvaa immunologista vastetta. Synteettinen syöpäsoluihin kohdentuva peptide, LXY30 sidottiin click-kemian avulla 573-kysteiiniin. Muokatut nanokapsidit myös leimattiin fluoresoivalla Cy5.5-värillä sitoen ne kapsidin primäärisiin aminehin. LXY30-muokattu nanopaksidi sitoutui spesifisesti syöpäsoluihin ja hiirimallissa syöpäsolu-xenokraftiin kun taas peptidiä sisältämätön kapsidi ei sitoutunut spesifisesti syöpäsouihin. Signaali pysyi kudoksessa 24 h. Sekä spesifit kapsidit että kontrollikapsidit sitoutuivat jonkun verran epäspesifisesti maksaan, pernaan ja munuaisiin.

Seuraavassa osatyössä nanokapsidiin lisättyihin kysteiineihin sidottiin kultananoklustereita. Nämä nanoklusterit eroavat kolloidaalisesta kullasta rakenteensa ja käytettävyyden osalta. $Au_{102}(p\text{MBA})_{44}$ (Au_{102}) ja maleimidi-

funktionalisoitu Au_{102} (Au_{102}_C_6MI) konjugoitiin nanokapsideihin suoran ligandivaihdon ja maleimide-tioli-konjugaation avuilla. Au_{102}_C_6MI sitoutui tehokkaammin nanokapseihin kuin Au_{102}, mutta se myös aggregoitui hanakammin liuoksessa. $Au_{102:n}$ oletettiin sitoutuvan suoraan 573-kysteiiniin mutta C6-linkkeri-modifioidun klusterin sijainti oli epäselvä. Mallintamisella selvitettiin missä HEV-nanokapsidissa sijaitsisivat C6-linkkerimodifioidut kultaklusterit: todennäköisin kultaklusterin sijainti johtaisi renkaan muodostukseen 5-symmetria-akselin ympärillä. Kryo-elektronimikroskooppinen 3D- rakenne yksittäisen partikkelin rekonstruktiona varmensi kultaklusterien sijainnin 5-symmetria-akselin ympärillä. Työssä kerätty rakennedata auttaa tulevaisuuden ligandien suunnittelussa ja toteuttamisessa.

Viimeisessä osatyössä verrattiin luonnollista ja rekombinanttienterovirusvektoria ja pyrittiin selvittämään vaikuttavatko rakenne- tai eirakenneproteiinit virusten kohdentamiseen soluihin. Rekombinanttienterovirus rakennettiin Echovirus 1n (EV1) rakenneproteiineista ja saman enterovirus B-ryhmän toisen viruksen coxsackievirus B5:n (CVB5) eirakenteellisista proteiineista. Nämä virukset käyttävät eri reseptoreita solun pinnalla, EV1 $\alpha 2\beta 1$ -integriiniä ja CVB5 coxsackievirus- ja adenovirus-reseptoria (CAR) ja DAF-molekyyliä (decay accelerating factor). Infektiokinetiikkatutkimukset ja infektioiden jakautuminen lyyttiseen ja kroonistyyppiseen infektioon osoittivat, että virusten rakenneproteiinit olivat määrääviä näiden ominaisuuksien suhteen. Virusten reseptorien osuutta virusinfektiotyypissä testattiin CVB3- ja CVB5-virusten avulla. CVB5 sitoutuu sekä CAR- että DAF-molekyyleihin kun taas CVB3 vain CAR-molekyyliin. RD-soluissa on luonnostaan erittäin vähän CAR-reseptoria, mikä antoi mahdollisuuden selvittää DAF-reseptorin tärkeyttä kroonistyyppisessä infektiossa. Tutkimukset viittasivat DAF- ja CAR-reseptorien vaikuttavan eri tavalla viruksen infektiokinetiikkaan. Tutkimukset rekombinanttiviruksilla siis antoivat lisäymmärrystä virusten kohdentamiseen ja niiden sisäänmenon tehokkuuteen.

Tämä väitöskirja yhdisti virusten infektiomekanismien tutkimusta, viruspohjaisten nanopartikkelien synteesiä ja tuotti tietoa nanopartikkelien käytöstä diagnostisiin sovelluksiin. Tämä väitöskirja kehitti yksilölliseen hoitoon tarvittavan nanokapsidialustan ja antoi työkaluja sen lisäkehitykseen.

REFERENCES

Ackerson C.J., Sykes M.T. & Kornberg R.D. 2005. Defined DNA/nanoparticle conjugates. *Proc Natl Acad Sci U S A* 102: 13383-13385.

Ackerson C.J., Powell R.D. & Hainfeld J.F. 2010a. Site-specific biomolecule labeling with gold clusters. *Methods Enzymol* 481: 195-230.

Ackerson C.J., Jadzinsky P.D., Jensen G.J. & Kornberg R.D. 2006. Rigid, Specific, and Discrete Gold Nanoparticle/Antibody Conjugates. *J Am Chem Soc* 128: 2635-2640.

Ackerson C.J., Jadzinsky P.D., Sexton J.Z., Bushnell D.A. & Kornberg R.D. 2010b. Synthesis and bioconjugation of 2 and 3 nm-diameter gold nanoparticles. *Bioconjug Chem* 21: 214-218.

Albanese A., Tang P.S. & Chan W.C. 2012. The effect of nanoparticle size, shape, and surface chemistry on biological systems. *Annu Rev Biomed Eng* 14: 1-16.

Almeida J.P., Figueroa E.R. & Drezek R.A. 2014. Gold nanoparticle mediated cancer immunotherapy. *Nanomedicine* 10: 503-514.

Argo E., Gimenez B. & Cash P. 1992. Non-cytopathic infection of rhabdomyosarcoma cells by coxsackie B5 virus. *Arch Virol* 126: 215-229.

Azubel M. & Kornberg R.D. 2016. Synthesis of Water-Soluble, Thiolate-Protected Gold Nanoparticles Uniform in Size. *Nano Lett* 16: 3348-3351.

Bachmann M.F. & Jennings G.T. 2010. Vaccine delivery: a matter of size, geometry, kinetics and molecular patterns. *Nat Rev Immunol* 10: 787-796.

Bai X.C., McMullan G. & Scheres S.H. 2015. How cryo-EM is revolutionizing structural biology. *Trends Biochem Sci* 40: 49-57.

Bai X.C., Fernandez I.S., McMullan G. & Scheres S.H. 2013. Ribosome structures to near-atomic resolution from thirty thousand cryo-EM particles. *Elife* 2: e00461.

Bailey A.M., Mao Y., Zeng J., Holla V., Johnson A., Brusco L., Chen K., Mendelsohn J., Routbort M.J., Mills G.B. & Meric-Bernstam F. 2014. Implementation of biomarker-driven cancer therapy: existing tools and remaining gaps. *Discov Med* 17: 101-114.

Banobre-Lopez M., Teijeiro A. & Rivas J. 2013. Magnetic nanoparticle-based hyperthermia for cancer treatment. *Rep Pract Oncol Radiother* 18: 397-400.

Bañobre-López M., Teijeiro A. & Rivas J. 2013. Magnetic nanoparticle-based hyperthermia for cancer treatment. *Rep Pract Oncol Radiother* 18: 397-400.

Barwal I., Kumar R., Kateriya S., Dinda A.K. & Yadav S.C. 2016. Targeted delivery system for cancer cells consist of multiple ligands conjugated genetically modified CCMV capsid on doxorubicin GNPs complex. *Sci Rep* 6: 37096.

Baskar R., Dai J., Wenlong N., Yeo R. & Yeoh K.-W. 2014. Biological response of cancer cells to radiation treatment. *Frontiers in Molecular Biosciences* 1.

Basle E., Joubert N. & Pucheault M. 2010. Protein chemical modification on endogenous amino acids. *Chem Biol* 17: 213-227.

Bergelson J.M., Chan B.M., Finberg R.W. & Hemler M.E. 1993. The integrin VLA-2 binds echovirus 1 and extracellular matrix ligands by different mechanisms. *J Clin Invest* 92: 232-239.

Bernardes G.J.L., Chalker J.M., Errey J.C. & Davis B.G. 2008. Facile conversion of cysteine and alkyl cysteines to dehydroalanine on protein surfaces: versatile and switchable access to functionalized proteins. *J Am Chem Soc* 130: 5052-5053.

Birkhauser F.D., Studer U.E., Froehlich J.M., Triantafyllou M., Bains L.J., Petralia G., Vermathen P., Fleischmann A. & Thoeny H.C. 2013. Combined ultrasmall superparamagnetic particles of iron oxide-enhanced and diffusion-weighted magnetic resonance imaging facilitates detection of metastases in normal-sized pelvic lymph nodes of patients with bladder and prostate cancer. *Eur Urol* 64: 953-960.

Blum A.S., Soto C.M., Wilson C.D., Cole J.D., Kim M., Gnade B., Chatterji A., Ochoa W.F., Lin T., Johnson J.E. & Ratna B.R. 2004. Cowpea Mosaic Virus as a Scaffold for 3-D Patterning of Gold Nanoparticles. *Nano Letters* 4: 867-870.

Bouslama L., Nasri D., Chollet L., Belguith K., Bourlet T., Aouni M., Pozzetto B. & Pillet S. 2007. Natural recombination event within the capsid genomic region leading to a chimeric strain of human enterovirus B. *J Virol* 81: 8944-8952.

Brannon-Peppas L. & Blanchette J.O. 2004. Nanoparticle and targeted systems for cancer therapy. *Adv Drug Deliv Rev* 56: 1649-1659.

Buonaguro L., Tagliamonte M., Visciano M.L., Tornesello M.L. & Buonaguro F.M. 2013. Developments in virus-like particle-based vaccines for HIV. *Expert Rev Vaccines* 12: 119-127.

Cal P.M.S.D., Bernardes G.J.L. & Gois P.M.P. 2014. Cysteine-Selective Reactions for Antibody Conjugation. *Angewandte Chemie International Edition* 53: 10585-10587.

Caldorera-Moore M.E., Liechty W.B. & Peppas N.A. 2011. Responsive theranostic systems: integration of diagnostic imaging agents and responsive controlled release drug delivery carriers. *Acc Chem Res* 44: 1061-1070.

Carson S.D., Chapman N.M., Hafenstein S. & Tracy S. 2011. Variations of coxsackievirus B3 capsid primary structure, ligands, and stability are selected for in a coxsackievirus and adenovirus receptor-limited environment. *J Virol* 85: 3306-3314.

Chalker J.M., Bernardes G.J., Lin Y.A. & Davis B.G. 2009. Chemical modification of proteins at cysteine: opportunities in chemistry and biology. *Chem Asian J* 4: 630-640.

Chao C.N., Lin M.C., Fang C.Y., Chen P.L., Chang D., Shen C.H. & Wang M. 2016. Gene Therapy for Human Lung Adenocarcinoma Using a Suicide Gene Driven by a Lung-Specific Promoter Delivered by JC Virus-Like Particles. *PLoS One* 11: e0157865.

Chapman N.M., Kim K.S., Drescher K.M., Oka K. & Tracy S. 2008. 5' terminal deletions in the genome of a coxsackievirus B2 strain occurred naturally in human heart. *Virology* 375: 480-491.

Chapman P.B., Hauschild A., Robert C., Haanen J.B., Ascierto P., Larkin J., Dummer R., Garbe C., Testori A., Maio M., Hogg D., Lorigan P., Lebbe C., Jouary T., Schadendorf D., Ribas A., O'Day S.J., Sosman J.A., Kirkwood J.M., Eggermont A.M., Dreno B., Nolop K., Li J., Nelson B., Hou J., Lee R.J., Flaherty K.T., McArthur G.A. & Group B.-S. 2011. Improved survival with vemurafenib in melanoma with BRAF V600E mutation. *N Engl J Med* 364: 2507-2516.

Charron D.M., Chen J. & Zheng G. 2015. Theranostic lipid nanoparticles for cancer medicine. *Cancer Treat Res* 166: 103-127.

Chen L.S., Wang M., Ou W.C., Fung C.Y., Chen P.L., Chang C.F., Huang W.S., Wang J.Y., Lin P.Y. & Chang D. 2010. Efficient gene transfer using the human JC virus-like particle that inhibits human colon adenocarcinoma growth in a nude mouse model. *Gene Ther* 17: 1033-1041.

Chen X., Chen Y., Yan M. & Qiu M. 2012. Nanosecond photothermal effects in plasmonic nanostructures. *ACS Nano* 6: 2550-2557.

Cheng R.H. & Xing L. 2014. *Proteolysis-resistant capsid of chimeric hepatitis E virus as an oral delivery vector*. The Regents Of The University Of California.

Cheng R.H., Xing L., Chen C.C. & STARK M.C. 2016. *Chemically activated nanocapsid functionalized for cancer targeting*. Google Patents.

Cheng Y. 2015. Single-particle cryo-EM at crystallographic resolution. *Cell* 161: 450-457.

Choi Y., Gyoo Park S., Yoo J.H. & Jung G. 2005. Calcium ions affect the hepatitis B virus core assembly. *Virology* 332: 454-463.

Cole A.J., Yang V.C. & David A.E. 2011. Cancer theranostics: the rise of targeted magnetic nanoparticles. *Trends Biotechnol* 29: 323-332.

Daniel M.C. & Astruc D. 2004. Gold nanoparticles: assembly, supramolecular chemistry, quantum-size-related properties, and applications toward biology, catalysis, and nanotechnology. *Chem Rev* 104: 293-346.

Daraee H., Eatemadi A., Abbasi E., Fekri Aval S., Kouhi M. & Akbarzadeh A. 2016. Application of gold nanoparticles in biomedical and drug delivery. *Artificial Cells, Nanomedicine, and Biotechnology* 44: 410-422.

Date A.A., Hanes J. & Ensign L.M. 2016. Nanoparticles for oral delivery: Design, evaluation and state-of-the-art. *J Control Release* 240: 504-526.

De Mattos-Arruda L., Dienstmann R. & Tabernero J. 2011. Development of molecular biomarkers in individualized treatment of colorectal cancer. *Clin Colorectal Cancer* 10: 279-289.

Desgrosellier J.S. & Cheresh D.A. 2010. Integrins in cancer: biological implications and therapeutic opportunities. *Nat Rev Cancer* 10: 9-22.

Dietel M., Johrens K., Laffert M.V., Hummel M., Blaker H., Pfitzner B.M., Lehmann A., Denkert C., Darb-Esfahani S., Lenze D., Heppner F.L., Koch A., Sers C., Klauschen F. & Anagnostopoulos I. 2015. A 2015 update on predictive molecular pathology and its role in targeted cancer therapy: a review focussing on clinical relevance. *Cancer Gene Ther* 22: 417-430.

Espinosa A., Di Corato R., Kolosnjaj-Tabi J., Flaud P., Pellegrino T. & Wilhelm C. 2016. Duality of Iron Oxide Nanoparticles in Cancer Therapy: Amplification of Heating Efficiency by Magnetic Hyperthermia and Photothermal Bimodal Treatment. *ACS Nano* 10: 2436-2446.

Farokhzad O.C. & Langer R. 2009. Impact of nanotechnology on drug delivery. *ACS Nano* 3: 16-20.

Frank J. 2017. Advances in the field of single-particle cryo-electron microscopy over the last decade. *Nat Protoc* 12: 209-212.

Ghaghada K.B., Starosolski Z.A., Lakoma A., Kaffes C., Agarwal S., Athreya K.K., Shohet J., Kim E. & Annapragada A. 2016. Heterogeneous Uptake of Nanoparticles in Mouse Models of Pediatric High-Risk Neuroblastoma. *PLoS One* 11: e0165877.

Gomez-Sebastian S., Lopez-Vidal J. & Escribano J.M. 2014. Significant productivity improvement of the baculovirus expression vector system by engineering a novel expression cassette. *PLoS One* 9: e96562.

Goossens N., Nakagawa S., Sun X. & Hoshida Y. 2015. Cancer biomarker discovery and validation. *Transl Cancer Res* 4: 256-269.

Greish K. 2007. Enhanced permeability and retention of macromolecular drugs in solid tumors: a royal gate for targeted anticancer nanomedicines. *J Drug Target* 15: 457-464.

Greish K. 2010. Enhanced permeability and retention (EPR) effect for anticancer nanomedicine drug targeting. *Methods Mol Biol* 624: 25-37.

Griffiths G. & Lucocq J.M. 2014. Antibodies for immunolabeling by light and electron microscopy: not for the faint hearted. *Histochem Cell Biol* 142: 347-360.

Gullberg M., Tolf C., Jonsson N., Mulders M.N., Savolainen-Kopra C., Hovi T., Van Ranst M., Lemey P., Hafenstein S. & Lindberg A.M. 2010a. Characterization of a putative ancestor of coxsackievirus B5. *J Virol* 84: 9695-9708.

Gullberg M., Tolf C., Jonsson N., Polacek C., Precechtelova J., Badurova M., Sojka M., Mohlin C., Israelsson S., Johansson K., Bopegamage S., Hafenstein S. & Lindberg A.M. 2010b. A single coxsackievirus B2 capsid residue controls cytolysis and apoptosis in rhabdomyosarcoma cells. *J Virol* 84: 5868-5879.

Guo F. & Jiang W. 2014. Single particle cryo-electron microscopy and 3-D reconstruction of viruses. *Methods Mol Biol* 1117: 401-443.

Guu T.S., Liu Z., Ye Q., Mata D.A., Li K., Yin C., Zhang J. & Tao Y.J. 2009. Structure of the hepatitis E virus-like particle suggests mechanisms for virus assembly and receptor binding. *Proc Natl Acad Sci U S A* 106: 12992-12997.

Hakkinen H., Walter M. & Gronbeck H. 2006. Divide and protect: capping gold nanoclusters with molecular gold-thiolate rings. *J Phys Chem B* 110: 9927-9931.

Han L., Wang W., Lu J., Kong F., Ma G., Zhu Y., Zhao D., Zhu J., Shuai W., Zhou Q., Chen P., Ye L., Tao J., Ahmad S., Li F. & Sun J. 2014. AAV-sBTLA facilitates HSP70 vaccine-triggered prophylactic antitumor

immunity against a murine melanoma pulmonary metastasis model in vivo. *Cancer Lett* 354: 398-406.

Hare J.I., Lammers T., Ashford M.B., Puri S., Storm G. & Barry S.T. 2017. Challenges and strategies in anti-cancer nanomedicine development: An industry perspective. *Adv Drug Deliv Rev* 108: 25-38.

Hasbrouck N.C. & High K.A. 2008. AAV-mediated gene transfer for the treatment of hemophilia B: problems and prospects. *Gene Ther* 15: 870-875.

Henke A., Launhardt H., Klement K., Stelzner A., Zell R. & Munder T. 2000. Apoptosis in coxsackievirus B3-caused diseases: interaction between the capsid protein VP2 and the proapoptotic protein siva. *J Virol* 74: 4284-4290.

Henry N.L. & Hayes D.F. 2012. Cancer biomarkers. *Mol Oncol* 6: 140-146.

Hervault A. & Thanh N.T. 2014. Magnetic nanoparticle-based therapeutic agents for thermo-chemotherapy treatment of cancer. *Nanoscale* 6: 11553-11573.

Horowitz E.D., Weinberg M.S. & Asokan A. 2011. Glycated AAV vectors: chemical redirection of viral tissue tropism. *Bioconjug Chem* 22: 529-532.

Hu M., Petrova H., Chen J., McLellan J.M., Siekkinen A.R., Marquez M., Li X., Xia Y. & Hartland G.V. 2006. Ultrafast laser studies of the photothermal properties of gold nanocages. *J Phys Chem B* 110: 1520-1524.

Huang X., Bronstein L.M., Retrum J., Dufort C., Tsvetkova I., Aniagyei S., Stein B., Stucky G., McKenna B., Remmes N., Baxter D., Kao C.C. & Dragnea B. 2007. Self-assembled virus-like particles with magnetic cores. *Nano Lett* 7: 2407-2416.

Hulkko E., Lopez-Acevedo O., Koivisto J., Levi-Kalisman Y., Kornberg R.D., Pettersson M. & Hakkinen H. 2011. Electronic and Vibrational Signatures of the Au-102(p-MBA)(44) Cluster. *J Am Chem Soc* 133: 3752-3755.

Jadzinsky P.D., Calero G., Ackerson C.J., Bushnell D.A. & Kornberg R.D. 2007. Structure of a thiol monolayer-protected gold nanoparticle at 1.1 A resolution. *Science* 318: 430-433.

Jariyapong P., Xing L., van Houten N.E., Li T.C., Weerachatyanukul W., Hsieh B., Moscoso C.G., Chen C.C., Niikura M. & Cheng R.H. 2013. Chimeric hepatitis E virus-like particle as a carrier for oral-delivery. *Vaccine* 31: 417-424.

Jo S.D., Ku S.H., Won Y.Y., Kim S.H. & Kwon I.C. 2016. Targeted Nanotheranostics for Future Personalized Medicine: Recent Progress in Cancer Therapy. *Theranostics* 6: 1362-1377.

Jobsri J., Allen A., Rajagopal D., Shipton M., Kanyuka K., Lomonossoff G.P., Ottensmeier C., Diebold S.S., Stevenson F.K. & Savelyeva N. 2015. Plant virus particles carrying tumour antigen activate TLR7 and Induce high levels of protective antibody. *PLoS One* 10: e0118096.

Jokinen J., White D.J., Salmela M., Huhtala M., Kapyla J., Sipila K., Puranen J.S., Nissinen L., Kankaanpaa P., Marjomaki V., Hyypia T., Johnson M.S. & Heino J. 2010. Molecular mechanism of alpha2beta1 integrin interaction with human echovirus 1. *EMBO J* 29: 196-208.

Jonsson N., Sävneby A., Gullberg M., Evertsson K., Klingel K. & Lindberg A.M. 2015a. Efficient replication of recombinant Enterovirus B types, carrying different P1 genes in the coxsackievirus B5 replicative backbone. *Virus Genes*: 1-7.

Jonsson N., Savneby A., Gullberg M., Evertsson K., Klingel K. & Lindberg A.M. 2015b. Efficient replication of recombinant Enterovirus B types, carrying different P1 genes in the coxsackievirus B5 replicative backbone. *Virus Genes* 50: 351-357.

Kamar N., Dalton H.R., Abravanel F. & Izopet J. 2014. Hepatitis E virus infection. *Clin Microbiol Rev* 27: 116-138.

Kamar N., Abravanel F., Lhomme S., Rostaing L. & Izopet J. 2015. Hepatitis E virus: chronic infection, extra-hepatic manifestations, and treatment. *Clin Res Hepatol Gastroenterol* 39: 20-27.

Kang H., Mintri S., Menon A.V., Lee H.Y., Choi H.S. & Kim J. 2015. Pharmacokinetics, pharmacodynamics and toxicology of theranostic nanoparticles. *Nanoscale* 7: 18848-18862.

Key J. & Leary J.F. 2014. Nanoparticles for multimodal in vivo imaging in nanomedicine. *International Journal of Nanomedicine* 9: 711-726.

Kim S., Park J.W., Kim D., Kim D., Lee I.H. & Jon S. 2009. Bioinspired colorimetric detection of calcium(II) ions in serum using calsequestrin-functionalized gold nanoparticles. *Angew Chem Int Ed Engl* 48: 4138-4141.

Kim S.H., Lee K.Y. & Jang Y.S. 2012. Mucosal Immune System and M Cell-targeting Strategies for Oral Mucosal Vaccination. *Immune Netw* 12: 165-175.

Knudsen K.B., Northeved H., Kumar Ek P., Permin A., Gjetting T., Andresen T.L., Larsen S., Wegener K.M., Lykkesfeldt J., Jantzen K., Loft S., Møller P. & Roursgaard M. 2015. In vivo toxicity of cationic micelles and liposomes. *Nanomedicine: Nanotechnology, Biology and Medicine* 11: 467-477.

Koivisto J., Chen X., Donnini S., Lahtinen T., Hakkinen H., Groenhof G. & Pettersson M. 2016. Acid-Base Properties and Surface Charge Distribution of the Water-Soluble Au-102(pMBA)(44) Nanocluster. *Journal of Physical Chemistry C* 120: 10041-10050.

Lahtinen T., Hulkko E., Sokołowska K., Tero T.-R., Saarnio V., Lindgren J., Pettersson M., Häkkinen H. & Lehtovaara L. 2016. Covalently linked multimers of gold nanoclusters Au102(p-MBA)44 and Au~250(p-MBA)n. *Nanoscale* 8: 18665-18674.

Lam K.S., Lebl M. & Krchnak V. 1997. The "One-Bead-One-Compound" Combinatorial Library Method. *Chem Rev* 97: 411-448.

Lammers T., Peschke P., Kuhnlein R., Subr V., Ulbrich K., Debus J., Huber P., Hennink W. & Storm G. 2007. Effect of radiotherapy and hyperthermia on the tumor accumulation of HPMA copolymer-based drug delivery systems. *J Control Release* 117: 333-341.

Laurent S., Saei A.A., Behzadi S., Panahifar A. & Mahmoudi M. 2014. Superparamagnetic iron oxide nanoparticles for delivery of therapeutic

agents: opportunities and challenges. *Expert Opinion on Drug Delivery* 11: 1449-1470.

Lee G.K., Maheshri N., Kaspar B. & Schaffer D.V. 2005. PEG conjugation moderately protects adeno-associated viral vectors against antibody neutralization. *Biotechnol Bioeng* 92: 24-34.

Ley K., Rivera-Nieves J., Sandborn W.J. & Shattil S. 2016. Integrin-based therapeutics: biological basis, clinical use and new drugs. *Nat Rev Drug Discov* 15: 173-183.

Li S.-W., Zhang J., He Z.-Q., Gu Y., Liu R.-S., Lin J., Chen Y.-X., Ng M.-H. & Xia N.-S. 2005a. Mutational Analysis of Essential Interactions Involved in the Assembly of Hepatitis E Virus Capsid. *J Biol Chem* 280: 3400-3406.

Li S.D. & Huang L. 2008. Pharmacokinetics and biodistribution of nanoparticles. *Mol Pharm* 5: 496-504.

Li S.W., Zhao Q., Wu T., Chen S., Zhang J. & Xia N.S. 2015. The development of a recombinant hepatitis E vaccine HEV 239. *Hum Vaccin Immunother* 11: 908-914.

Li S.W., Zhang J., Li Y.M., Ou S.H., Huang G.Y., He Z.Q., Ge S.X., Xian Y.L., Pang S.Q., Ng M.H. & Xia N.S. 2005b. A bacterially expressed particulate hepatitis E vaccine: antigenicity, immunogenicity and protectivity on primates. *Vaccine* 23: 2893-2901.

Li T.C., Yamakawa Y., Suzuki K., Tatsumi M., Razak M.A., Uchida T., Takeda N. & Miyamura T. 1997. Expression and self-assembly of empty virus-like particles of hepatitis E virus. *J Virol* 71: 7207-7213.

Li Y., Xiao K., Luo J., Lee J., Pan S. & Lam K.S. 2010. A novel size-tunable nanocarrier system for targeted anticancer drug delivery. *J Control Release* 144: 314-323.

Lizotte P.H., Wen A.M., Sheen M.R., Fields J., Rojanasopondist P., Steinmetz N.F. & Fiering S. 2016. In situ vaccination with cowpea mosaic virus nanoparticles suppresses metastatic cancer. *Nat Nanotechnol* 11: 295-303.

Lopez-Vidal J., Gomez-Sebastian S., Barcena J., Nunez Mdel C., Martinez-Alonso D., Dudognon B., Guijarro E. & Escribano J.M. 2015. Improved Production Efficiency of Virus-Like Particles by the Baculovirus Expression Vector System. *PLoS One* 10: e0140039.

Luque-Michel E., Imbuluzqueta E., Sebastian V. & Blanco-Prieto M.J. 2016. Clinical advances of nanocarrier-based cancer therapy and diagnostics. *Expert Opin Drug Deliv*.

Lyon R.P., Setter J.R., Bovee T.D., Doronina S.O., Hunter J.H., Anderson M.E., Balasubramanian C.L., Duniho S.M., Leiske C.I., Li F. & Senter P.D. 2014. Self-hydrolyzing maleimides improve the stability and pharmacological properties of antibody-drug conjugates. *Nat Biotechnol* 32: 1059-1062.

Marjomaki V., Turkki P. & Huttunen M. 2015. Infectious Entry Pathway of Enterovirus B Species. *Viruses* 7: 6387-6399.

Marjomaki V., Lahtinen T., Martikainen M., Koivisto J., Malola S., Salorinne K., Pettersson M. & Hakkinen H. 2014. Site-specific targeting of enterovirus capsid by functionalized monodisperse gold nanoclusters. *Proc Natl Acad Sci U S A* 111: 1277-1281.

Markides H., Rotherham M. & El Haj A.J. 2012. Biocompatibility and Toxicity of Magnetic Nanoparticles in Regenerative Medicine. *Journal of Nanomaterials* 2012: e614094.

Masuda T., Akita H., Niikura K., Nishio T., Ukawa M., Enoto K., Danev R., Nagayama K., Ijiro K. & Harashima H. 2009. Envelope-type lipid nanoparticles incorporating a short PEG-lipid conjugate for improved control of intracellular trafficking and transgene transcription. *Biomaterials* 30: 4806-4814.

McDermott U. & Settleman J. 2009. Personalized cancer therapy with selective kinase inhibitors: an emerging paradigm in medical oncology. *J Clin Oncol* 27: 5650-5659.

Miller A.D. 2013. Lipid-based nanoparticles in cancer diagnosis and therapy. *J Drug Deliv* 2013: 165981.

Milstone A.M., Petrella J., Sanchez M.D., Mahmud M., Whitbeck J.C. & Bergelson J.M. 2005. Interaction with coxsackievirus and adenovirus receptor, but not with decay-accelerating factor (DAF), induces A-particle formation in a DAF-binding coxsackievirus B3 isolate. *J Virol* 79: 655-660.

Minor P.D. 2004. Polio eradication, cessation of vaccination and re-emergence of disease. *Nat Rev Microbiol* 2: 473-482.

Molino N.M., Anderson A.K., Nelson E.L. & Wang S.W. 2013. Biomimetic protein nanoparticles facilitate enhanced dendritic cell activation and cross-presentation. *ACS Nano* 7: 9743-9752.

Muehlenbachs A., Bhatnagar J. & Zaki S.R. 2015. Tissue tropism, pathology and pathogenesis of enterovirus infection. *J Pathol* 235: 217-228.

Mura S. & Couvreur P. 2012. Nanotheranostics for personalized medicine. *Adv Drug Deliv Rev* 64: 1394-1416.

Negishi Y., Nobusada K. & Tsukuda T. 2005. Glutathione-protected gold clusters revisited: bridging the gap between gold(I)-thiolate complexes and thiolate-protected gold nanocrystals. *J Am Chem Soc* 127: 5261-5270.

Niikura M., Takamura S., Kim G., Kawai S., Saijo M., Morikawa S., Kurane I., Li T.C., Takeda N. & Yasutomi Y. 2002. Chimeric recombinant hepatitis E virus-like particles as an oral vaccine vehicle presenting foreign epitopes. *Virology* 293: 273-280.

Oberste M.S., Maher K., Kilpatrick D.R. & Pallansch M.A. 1999a. Molecular evolution of the human enteroviruses: correlation of serotype with VP1 sequence and application to picornavirus classification. *J Virol* 73: 1941-1948.

Oberste M.S., Maher K., Kilpatrick D.R., Flemister M.R., Brown B.A. & Pallansch M.A. 1999b. Typing of human enteroviruses by partial sequencing of VP1. *J Clin Microbiol* 37: 1288-1293.

Orlov I., Schertel A., Zuber G., Klaholz B., Drillien R., Weiss E., Schultz P. & Spehner D. 2015. Live cell immunogold labelling of RNA polymerase II. *Sci Rep* 5: 8324.

Peng J.M., Liang S.M. & Liang C.M. 2004. VP1 of foot-and-mouth disease virus induces apoptosis via the Akt signaling pathway. *J Biol Chem* 279: 52168-52174.

Plotkin S.A. 2005. Vaccines: past, present and future. *Nat Med* 11: S5-11.

Powell R.D. & Hainfeld J.F. 2011. Preparation and high-resolution microscopy of gold cluster labeled nucleic acid conjugates and nanodevices. *Micron (Oxford, England : 1993)* 42: 163-174.

Rintanen N., Karjalainen M., Alanko J., Paavolainen L., Maki A., Nissinen L., Lehkonen M., Kallio K., Cheng R.H., Upla P., Ivaska J. & Marjomaki V. 2012. Calpains promote alpha2beta1 integrin turnover in nonrecycling integrin pathway. *Mol Biol Cell* 23: 448-463.

Salorinne K., Lahtinen T., Malola S., Koivisto J. & Hakkinen H. 2014. Solvation chemistry of water-soluble thiol-protected gold nanocluster Au(1)(0)(2) from DOSY NMR spectroscopy and DFT calculations. *Nanoscale* 6: 7823-7826.

Santio N.M., Salmela M., Arola H., Eerola S.K., Heino J., Rainio E.M. & Koskinen P.J. 2016. The PIM1 kinase promotes prostate cancer cell migration and adhesion via multiple signalling pathways. *Exp Cell Res* 342: 113-124.

Savneby A., Luthman J., Nordenskjold F., Andersson B. & Lindberg A.M. 2016. The Transcriptome of Rhabdomyosarcoma Cells Infected with Cytolytic and Non-Cytolytic Variants of Coxsackievirus B2 Ohio-1. *PLoS One* 11: e0164548.

Seow Y. & Wood M.J. 2009. Biological Gene Delivery Vehicles: Beyond Viral Vectors. *Molecular Therapy: the Journal of the American Society of Gene Therapy* 17: 767-777.

Sexton J.Z. & Ackerson C.J. 2010. Determination of Rigidity of Protein Bound Au(144) Clusters by Electron Cryomicroscopy. *J Phys Chem C Nanomater Interfaces* 114: 16037-16042.

Shigematsu H. & Sigworth F.J. 2013. Noise models and cryo-EM drift correction with a direct-electron camera. *Ultramicroscopy* 131: 61-69.

Shima R., Li T.C., Sendai Y., Kataoka C., Mori Y., Abe T., Takeda N., Okamoto T. & Matsuura Y. 2016. Production of hepatitis E virus-like particles presenting multiple foreign epitopes by co-infection of recombinant baculoviruses. *Sci Rep* 6: 21638.

Simmonds P. 2006. Recombination and selection in the evolution of picornaviruses and other Mammalian positive-stranded RNA viruses. *J Virol* 80: 11124-11140.

Sperling R.A., Rivera Gil P., Zhang F., Zanella M. & Parak W.J. 2008. Biological applications of gold nanoparticles. *Chem Soc Rev* 37: 1896-1908.

Srinivasarao M., Galliford C.V. & Low P.S. 2015. Principles in the design of ligand-targeted cancer therapeutics and imaging agents. *Nat Rev Drug Discov* 14: 203-219.

Stapleton S., Jaffray D. & Milosevic M. 2017a. Radiation effects on the tumor microenvironment: Implications for nanomedicine delivery. *Adv Drug Deliv Rev* 109: 119-130.

Stapleton S.J., Valerio T.D., Astroth K. & Woodhouse S. 2017b. Distress During Radiation Therapy: Assessment Among Patients With Breast or Prostate Cancer. *Clin J Oncol Nurs* 21: 93-98.

Steinmetz N.F., Evans D.J. & Lomonossoff G.P. 2007. Chemical Introduction of Reactive Thiols Into a Viral Nanoscaffold: A Method that Avoids Virus Aggregation. *Chembiochem* 8: 1131-1136.

Stephanopoulos N. & Francis M.B. 2011. Choosing an effective protein bioconjugation strategy. *Nat Chem Biol* 7: 876-884.

Strable E. & Finn M.G. 2009. Chemical modification of viruses and virus-like particles. *Curr Top Microbiol Immunol* 327: 1-21.

Subbaram S. & Dipersio C.M. 2011. Integrin alpha3beta1 as a breast cancer target. *Expert Opin Ther Targets* 15: 1197-1210.

Takamura S., Niikura M., Li T.C., Takeda N., Kusagawa S., Takebe Y., Miyamura T. & Yasutomi Y. 2004. DNA vaccine-encapsulated virus-like particles derived from an orally transmissible virus stimulate mucosal and systemic immune responses by oral administration. *Gene Ther* 11: 628-635.

Tam A.W., Smith M.M., Guerra M.E., Huang C.C., Bradley D.W., Fry K.E. & Reyes G.R. 1991. Hepatitis E virus (HEV): molecular cloning and sequencing of the full-length viral genome. *Virology* 185: 120-131.

Thanki K., Gangwal R.P., Sangamwar A.T. & Jain S. 2013. Oral delivery of anticancer drugs: challenges and opportunities. *J Control Release* 170: 15-40.

Tissot A.C., Renhofa R., Schmitz N., Cielens I., Meijerink E., Ose V., Jennings G.T., Saudan P., Pumpens P. & Bachmann M.F. 2010. Versatile virus-like particle carrier for epitope based vaccines. *PLoS One* 5: e9809.

Upla P., Marjomaki V., Kankaanpaa P., Ivaska J., Hyypia T., Van Der Goot F.G. & Heino J. 2004. Clustering induces a lateral redistribution of alpha 2 beta 1 integrin from membrane rafts to caveolae and subsequent protein kinase C-dependent internalization. *Mol Biol Cell* 15: 625-636.

van Oers M.M., Pijlman G.P. & Vlak J.M. 2015. Thirty years of baculovirus-insect cell protein expression: from dark horse to mainstream technology. *J Gen Virol* 96: 6-23.

Wang C.Y., Miyazaki N., Yamashita T., Higashiura A., Nakagawa A., Li T.C., Takeda N., Xing L., Hjalmarsson E., Friberg C., Liou D.M., Sung Y.J., Tsukihara T., Matsuura Y., Miyamura T. & Cheng R.H. 2008. Crystallization and preliminary X-ray diffraction analysis of recombinant hepatitis E virus-like particle. *Acta Crystallogr Sect F Struct Biol Cryst Commun* 64: 318-322.

Wang F., Liu X., Lu C.H. & Willner I. 2013. Cysteine-mediated aggregation of Au nanoparticles: the development of a H2O2 sensor and oxidase-based biosensors. *ACS Nano* 7: 7278-7286.

Wang Q., Lin T., Johnson J.E. & Finn M.G. 2002. Natural supramolecular building blocks. Cysteine-added mutants of cowpea mosaic virus. *Chem Biol* 9: 813-819.

Wareing M.D. & Tannock G.A. 2001. Live attenuated vaccines against influenza; an historical review. *Vaccine* 19: 3320-3330.

Wu X., Chen P., Lin H., Hao X. & Liang Z. 2016. Hepatitis E virus: Current epidemiology and vaccine. *Hum Vaccin Immunother* 12: 2603-2610.

Wust P., Hildebrandt B., Sreenivasa G., Rau B., Gellermann J., Riess H., Felix R. & Schlag P.M. 2002. Hyperthermia in combined treatment of cancer. *Lancet Oncol* 3: 487-497.

Xiao W., Wang Y., Lau E.Y., Luo J., Yao N., Shi C., Meza L., Tseng H., Maeda Y., Kumaresan P., Liu R., Lightstone F.C., Takada Y. & Lam K.S. 2010. The use of one-bead one-compound combinatorial library technology to discover high-affinity alphavbeta3 integrin and cancer targeting arginine-glycine-aspartic acid ligands with a built-in handle. *Mol Cancer Ther* 9: 2714-2723.

Xiao W., Li T., Bononi F.C., Lac D., Kekessie I.A., Liu Y., Sanchez E., Mazloom A., Ma A.-H., Lin J., Tran J., Yang K., Lam K.S. & Liu R. 2016. Discovery and characterization of a high-affinity and high-specificity peptide ligand LXY30 for in vivo targeting of α3 integrin-expressing human tumors. *EJNMMI research* 6: 18.

Xing L., Kato K., Li T., Takeda N., Miyamura T., Hammar L. & Cheng R.H. 1999. Recombinant hepatitis E capsid protein self-assembles into a dual-domain T = 1 particle presenting native virus epitopes. *Virology* 265: 35-45.

Xing L., Li T.C., Mayazaki N., Simon M.N., Wall J.S., Moore M., Wang C.Y., Takeda N., Wakita T., Miyamura T. & Cheng R.H. 2010. Structure of hepatitis E virion-sized particle reveals an RNA-dependent viral assembly pathway. *J Biol Chem* 285: 33175-33183.

Xing L., Wang J.C., Li T.C., Yasutomi Y., Lara J., Khudyakov Y., Schofield D., Emerson S.U., Purcell R.H., Takeda N., Miyamura T. & Cheng R.H. 2011. Spatial configuration of hepatitis E virus antigenic domain. *J Virol* 85: 1117-1124.

Xu X., Ho W., Zhang X., Bertrand N. & Farokhzad O. 2015. Cancer nanomedicine: from targeted delivery to combination therapy. *Trends Mol Med* 21: 223-232.

Yamashita T., Mori Y., Miyazaki N., Cheng R.H., Yoshimura M., Unno H., Shima R., Moriishi K., Tsukihara T., Li T.C., Takeda N., Miyamura T. & Matsuura Y. 2009. Biological and immunological characteristics of hepatitis E virus-like particles based on the crystal structure. *Proc Natl Acad Sci U S A* 106: 12986-12991.

Yang C., Pan H., Wei M., Zhang X., Wang N., Gu Y., Du H., Zhang J., Li S. & Xia N. 2013. Hepatitis E virus capsid protein assembles in 4M urea in the presence of salts. *Protein Sci* 22: 314-326.

Yi H., Strauss J.D., Ke Z., Alonas E., Dillard R.S., Hampton C.M., Lamb K.M., Hammonds J.E., Santangelo P.J., Spearman P.W. & Wright E.R. 2015. Native immunogold labeling of cell surface proteins and viral glycoproteins for cryo-electron microscopy and cryo-electron tomography applications. *J Histochem Cytochem* 63: 780-792.

Yu H., Li S., Yang C., Wei M., Song C., Zheng Z., Gu Y., Du H., Zhang J. & Xia N. 2011a. Homology model and potential virus-capsid binding site of a putative HEV receptor Grp78. *J Mol Model* 17: 987-995.

Yu Q., Zhang Y., Wang H., Brash J. & Chen H. 2011b. Anti-fouling bioactive surfaces. *Acta Biomater* 7: 1550-1557.

Yu S.L., Shi W.X., Lu Y. & Yang J.X. 2011c. Characterization and anti-fouling performance of nano-Al(2)O(3)/PVDF membrane for Songhua river raw water filtration. *Water Sci Technol* 64: 1892-1897.

Zautner A.E., Jahn B., Hammerschmidt E., Wutzler P. & Schmidtke M. 2006. N- and 6-O-sulfated heparan sulfates mediate internalization of coxsackievirus B3 variant PD into CHO-K1 cells. *J Virol* 80: 6629-6636.

Zeltz C., Brezillon S., Kapyla J., Eble J.A., Bobichon H., Terryn C., Perreau C., Franz C.M., Heino J., Maquart F.X. & Wegrowski Y. 2010. Lumican inhibits cell migration through alpha2beta1 integrin. *Exp Cell Res* 316: 2922-2931.

Zhang J., Pei Y., Zhang H., Wang L., Arrington L., Zhang Y., Glass A. & Leone A.M. 2013. Assessing the heterogeneity level in lipid nanoparticles for siRNA delivery: size-based separation, compositional heterogeneity, and impact on bioperformance. *Mol Pharm* 10: 397-405.

Zhang X.-D., Luo Z., Chen J., Song S., Yuan X., Shen X., Wang H., Sun Y., Gao K., Zhang L., Fan S., Leong D.T., Guo M. & Xie J. 2015. Ultrasmall Glutathione-Protected Gold Nanoclusters as Next Generation Radiotherapy Sensitizers with High Tumor Uptake and High Renal Clearance. *Sci Rep* 5: 8669.

Zhao Q., Li S., Yu H., Xia N. & Modis Y. 2013. Virus-like particle-based human vaccines: quality assessment based on structural and functional properties. *Trends Biotechnol* 31: 654-663.

Zhao Y., Wang C., Wang L., Yang Q., Tang W., She Z. & Deng Y. 2012. A frustrating problem: Accelerated blood clearance of PEGylated solid lipid nanoparticles following subcutaneous injection in rats. *Eur J Pharm Biopharm* 81: 506-513.

Zolnik B.S., Gonzalez-Fernandez A., Sadrieh N. & Dobrovolskaia M.A. 2010. Nanoparticles and the immune system. *Endocrinology* 151: 458-465.

ORIGINAL PAPERS

I

CHEMICALLY ACTIVATABLE VIRAL CAPSID FUNCTIONALIZED FOR CANCER TARGETING

by

Chun-Chieh Chen, Li Xing, Marie Stark, Tingwei Ou, Prasida Holla, Kai Xiao, Bruce D Hammock, Kit Lam, R Holland Cheng
Nanomedicine 11(4): 337–390.

II

SURFACE MODULATABLE NANOCAPSIDS FOR TARGETING AND TRACKING TOWARD NANOTHERANOSTIC DELIVERY

by

Marie Stark & R. Holland Cheng 2016

Pharmaceutical Patent Analyst 5(5), 307-317

III

STRUCTURAL CHARACTERIZATION OF SITE-MODULATED NANOCAPSID WITH MONODISPERSED GOLD CLUSTERS

by

Marie Stark, Mo Baikoghli & Tanja Lahtinen, Sami Malola, Li Xing, Michelle Nguyen, Marina Nguyen, Aria Sikaroudi, Varpu Marjomäki, Hannu Häkkinen, and R Holland Cheng

Submitted Manuscript to Scientific Reports May 2017

IV

ENTEROVIRUS PERSISTENCY IN RHABDOMYCOSARCOMA CELLS IS THE RESULT OF DEFECTIVE ENTRY TO CELLS

by

Paula Turkki, Marie C Stark, Anna Göransson, Mira Myllynen, Heidi Del-Maso Sallinen, Michael Lindberg, Varpu Marjomaki

Manuscript 2017